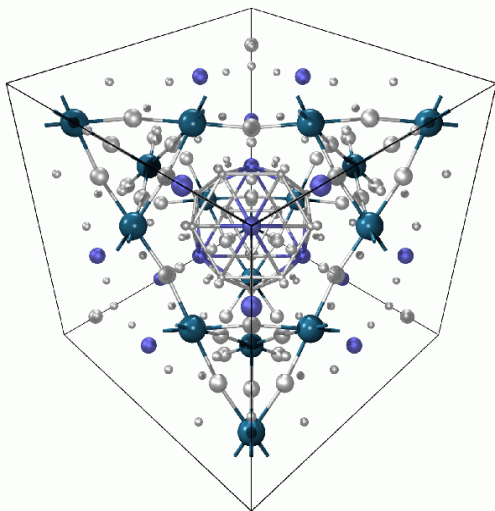


# NANOVED NANOTECH TECHTRANSFER



**e - Proceedings**

## **NANOVED & NANOTECH & TECHTRANSFER 2010**

**5th International Conference  
on Nanosciences, Nanotechnologies, Nanomaterials,  
Nanomedicine and Technology Transfer  
Bratislava, Slovakia, May 16 – 19, 2010**

# **NANOVED & NANOTECH & TECHTRANSFER 2010**

**5th International Conference  
on Nanosciences, Nanotechnologies, Nanomaterials,  
Nanomedicine and Technology Transfer  
Bratislava, Slovakia, May 16 – 19, 2010**

## **e - Proceedings**

**Editors:**

**Magdaléna Kadlečíková  
Filip Lazišťan  
Jozef Kadlečík  
Peter Švec**

**[www.nano2010.sk](http://www.nano2010.sk);      [www.nanoved2010.sk](http://www.nanoved2010.sk)**

## **OBSAH**

|  |           |
|--|-----------|
| <b>SYNTHESIS OF CARBON NANOSTRUCTURES BY PLASMA ENHANCED CHEMICAL VAPOUR DEPOSITION AT ATMOSPHERIC PRESSURE .....</b>                                      | <b>4</b>  |
| <b>COMPOSITE MATERIALS REINFORCED BY SHORT (NANO) FIBRES – COMPUTATIONAL SIMULATIONS .....</b>   | <b>8</b>  |
| <b>ROLE OF THE SLOVAK CENTRE OF SCIENTIFIC AND TECHNICAL INFORMATION IN THE SUPPORT OF RESEARCH, DEVELOPMENT, INNOVATION AND TECHNOLOGY TRANSFER .....</b> | <b>12</b> |
| <b>PROPERTIES OF FE-CO NANOPOWDER PREPARED BY CHEMICAL SYNTHESIS .....</b>   | <b>17</b> |
| <b>ZVIDITEĽŇOVANIE KRYŠTALOGRAFICKÝCH DEFEKTOV V GAP POMOCOU MOKRÉHO CHEMICKÉHO LEPTANIA .....</b>   | <b>21</b> |
| <b>POINT OF CARE TESTING ( POCT ), NANOTECHNOLÓGIE A PERSONALIZOVANÁ LABORATÓRNA DIAGNOSTIKA.....</b>  | <b>26</b> |
| <b>INDENTATION LOAD-SIZE EFFECT IN AL<sub>2</sub>O<sub>3</sub>-SiC NANOCOMPOSITES .....</b>  | <b>32</b> |
| <b>DETERMINATION OF PARTICLE SHAPE AND SIZE DISTRIBUTION OF MODEL TYPES OF NANOMATERIALS.....</b>  | <b>38</b> |
| <b>CARBON NANOTUBE BRIDGES GROWN ON ALUMINOSILICATES BY HOT FILAMENT CVD PROCESS .....</b>   | <b>42</b> |

# SYNTHESIS OF CARBON NANOSTRUCTURES BY PLASMA ENHANCED CHEMICAL VAPOUR DEPOSITION AT ATMOSPHERIC PRESSURE

*O. Jašek<sup>1</sup>, P. Synek<sup>2</sup>, L. Zajíčková<sup>1</sup>, M. Eliáš<sup>1</sup>, V. Kudrle<sup>1</sup>*

<sup>1</sup> *Department of Physical Electronics, Faculty of Science, Masaryk University, Kotlářská 2, 602 00 Brno, Czech Republic*

Corresponding author: jasek@physics.muni.cz

## **Abstract**

Carbon nanostructures present leading field in nanotechnology research. Wide range of chemical and physical methods was used for carbon nanostructures synthesis including arc discharges, laser ablation and chemical vapour deposition. Plasma enhanced chemical vapour deposition (PECVD) with its application in modern microelectronics industry became soon target of research in carbon nanostructures synthesis. The selection of the ideal growth process depends on the application. Most of PECVD techniques work at low pressure requiring vacuum systems. However for industrial applications it would be desirable to work at atmospheric pressure. In this article carbon nanostructures synthesis by plasma discharges working at atmospheric pressure will be reviewed. Special attention will be given to microwave discharges and atmospheric pressure glow discharge (APG). Our group has successfully synthesized multi-walled carbon nanotubes directly on substrate or in volume by microwave plasma torch. We were able to growth several tens of micrometers high layer of nanotubes in time less than 1 minute, without any external heating source. The carbon nanotubes layer could be also grown on substrates without a buffer layer or with predefined patterns. Lately APG discharge became an attractive method to growth single-walled carbon nanotubes with good alignment. Critical factor for growth of carbon nanotubes is the catalyst. Properties of buffer layer between substrate and catalyst and catalytic particles size considerably influence final product and are key to control of nanotube properties and growth conditions such as temperature and gas mixture. In the end of the article a possibility to synthesize graphene with atmospheric pressure discharges is discussed.

## **Introduction**

Carbon with its many allotropes became major player in nanotechnological research. From discovery of fullerenes [1], through carbon nanotubes [2] to the latest, but hopefully not last surprise, addition of graphene [3], stable 2-dimensional carbon structure, the nano research was electrified by carbon structures. Fullerene took the Nobel prize in 1996, carbon nanotubes are taking regularly first spot on number of published articles in field of nanotechnology to even more surprising and fascinating properties such a quantum Hall effect and electrons obeying Dirac equation of graphene. Synthesis of carbon nanostructure was closely related to plasma processes. Carbon nanotubes, similarly to fullerenes, could be synthesized by arc discharge [2], laser ablation [4] and chemical vapour deposition (CVD) [5] methods. For industrial applications, such as flat panel displays or field emitters, it is desirable to produce vertically aligned CNT films with uniform properties. The preparation of the aligned CNTs was reported by thermal, plasma enhanced and hot filament CVD methods [6]. Plasma enhanced CVD (PECVD) refers to the case where a plasma source is used to create a discharge. The introduction of the catalyst divides the CVD methods into the group of bulk production techniques using catalyst in the gas phase, so called floating catalyst methods, and surface-bound CVD with supported catalyst either in the form of catalyst nanoparticles [7] or ultrathin films [8]. Most of these techniques work at low pressure requiring vacuum systems. However for industrial applications it would be desirable to work at atmospheric pressure.

### ***Carbon nanotubes synthesis by PECVD at atmospheric pressure***

Recently, atmospheric pressure discharges have become studied by some research groups because of their relatively simple set-up without expensive vacuum systems. Some publications deal with the synthesis of CNTs using d.c. plasma arc jet or torch ignited in flow gas between two electrodes. This approach is close to the arc discharge method because it is based on evaporation of solid carbon introduced as one of the electrodes and/or powder [9]. The catalyst can be integrated into graphite electrode or introduced into the gas phase. Generally, these methods produce soot with certain portion of unaligned single and multi-walled CNTs. The experiments with microwave (mw) torches are focused on the floating catalyst approach (ferrocene, iron pentacarbonyl), i. e., also bulk production of unaligned CNTs [10]. On the other hand, the mw torch has been successfully used by our group for high speed synthesis of vertically aligned supported CNTs [11-12]. With regards the dielectric barrier discharges (DBDs), Kyung, Lee et al. investigated filamentary DBD discharges at kHz frequencies for the deposition of supported CNTs. They tested multipin electrode covered by the dielectric plate [13] and capillary dielectric barrier [14] configurations. The most successful application of DBD, in this case of its glow mode called atmospheric pressure glow (APG), was performed by Nozaki. Besides the growth of unaligned CNTs of low quality in APG driven at 125 kHz and the growth of CNFs in radio frequency (r.f.) APG, he showed the growth of vertically aligned SWNTs [15] in r.f. APG using He/H<sub>2</sub>/CH<sub>4</sub> feed.

Our group has grown CNTs in the atmospheric pressure microwave plasma torch directly on substrate. The microwave plasma torch apparatus consists of microwave generator working at the frequency of 2.45 GHz and standard rectangular waveguide transmitting the mw power through a coaxial line to a hollow nozzle electrode. Ferrite circulator protects the generator against the reflected power by rerouting it to the water load. The matching of the plasma load to the line impedance is achieved by a three stub matching unit. Working gas mixture flows through the central conductor of the coaxial line and the nozzle electrode. The central conductor is held in place by a boron nitride ceramics. The outer conductor of the coaxial line is terminated by a flange. Detailed drawing of the current set-up is in Fig. 1. , detail of deposition chamber Fig. 2. The standard deposition mixture consists of argon, methane and hydrogen. The coaxial line and the electrode accommodate a dual gas flow. Argon passes through the centre whereas the reactive mixture of hydrogen and methane is added by a concentric opening instead of the set of holes in the outer housing.

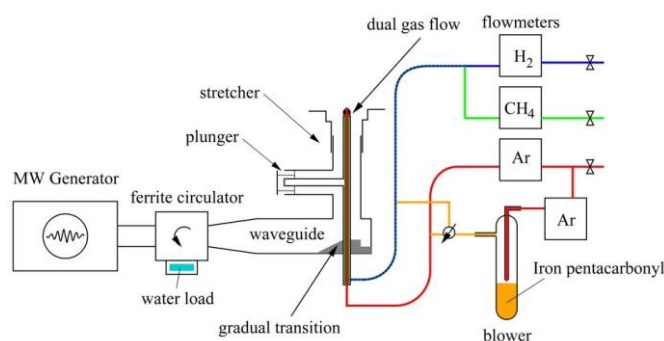


**Fig. 1.** Experimental apparatus scheme.

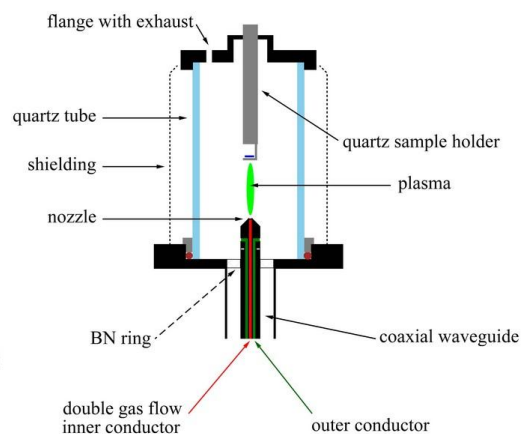


**Fig. 2.** Deposition chamber detail.

The plasma torch is enclosed by a quartz tube, 200 mm in length, and duralumin shielding is wrapped around the tube. The diameter of the quartz tube is 80 mm.

The substrate for MWNTs growth, silicon piece with the dimensions 10x15 mm<sup>2</sup>, was fixed on the quartz holder in the variable distance from the torch nozzle. It was heated by a heat exchange with hot gas and surface recombination. Therefore, its temperature was determined by power input, gas mixture and its distance from the nozzle. The mw power applied for the deposition of CNTs was 400 W. Argon flow rate was changed from 700 to 1500 sccm. Hydrogen flow rate was between 285 and 430 sccm, methane flow rate was 42 sccm. The catalyst was 1-15 nm thick iron film prepared by vacuum evaporation. The used substrates for deposition are Si, Si/SiO<sub>2</sub> or Si/Al<sub>2</sub>O<sub>3</sub> with the iron catalyst layer. Example of a such deposited carbon nanotube layer can be found on Fig.3. Deposited samples were studied by scanning and transmission electron microscopy and Raman spectroscopy.

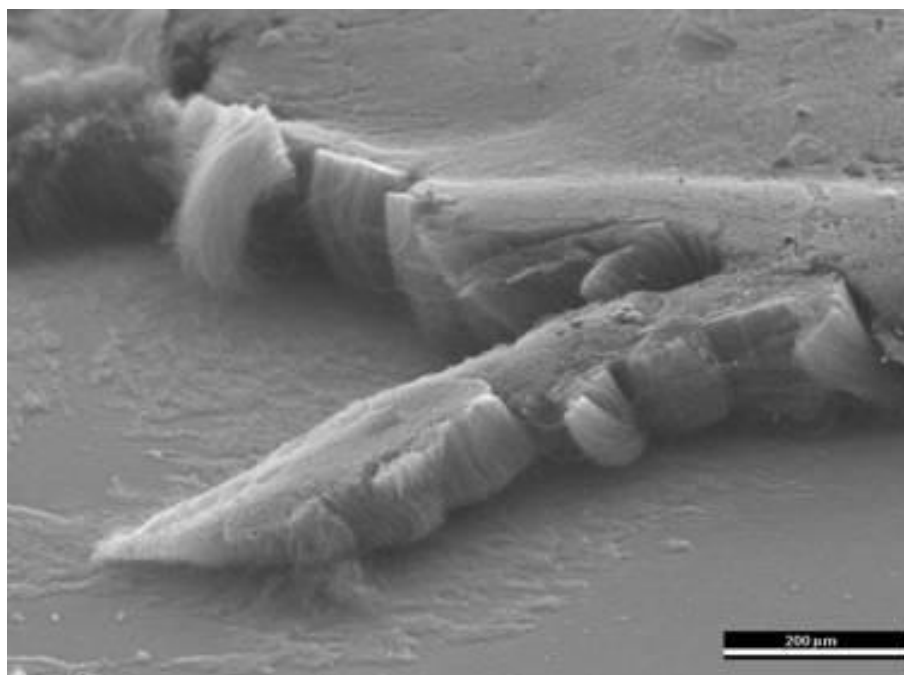


**Fig.3.** MWCNTs deposited on Si/SiO<sub>2</sub>/Fe substrate by microwave plasma torch.

### ***Catalyst role at the nanotube growth***

For the carbon nanotube growth it is necessary to obtain nanometer scale catalytic particles. Except a wide range of chemical methods, the catalytic particles can be directly generated by decomposition of organometallic compound (floating catalyst method) or by reconstructing thin layer of catalyst (surface bound catalyst method). The restructuring of ultrathin metallic films of catalysis for CNT growth is usually obtained by heating the films in N<sub>2</sub>, H<sub>2</sub> or NH<sub>3</sub> [16] or plasma treatment [17]. Thin films have a high surface-to-volume ratio and the heating results in the development of holes and, eventually, particles [18]. The particles can coalesce during continuous heating due to Ostwald ripening or surface migration [19], thus modifying the final distribution of catalytic particles. This process is strongly dependent on the heating time and gas environment [20], the thickness of the pristine catalytic layer [21] and its surface morphology [22]. In addition to this, the interaction with the material under the catalyst is of importance especially in case of integration on the Si substrates. Application of buffer layer between catalyst and substrate can hinder unwanted reaction and significantly enhance carbon nanotube growth. It was shown lately by several authors that careful reconstruction of catalyst layer under special conditions can be used to substantially lower deposition temperature of carbon nanotubes [23] or generated nanotubes with given electrical properties [24-25]. Usage of Al<sub>2</sub>O<sub>3</sub> buffer layer with combination of small amount H<sub>2</sub>O vapor also lead to discovery of so called super-growth technique [26], which can be use to grow several millimetres high nanotube forest in the matter of minutes.

### ***Graphene synthesis by PECVD at atmospheric pressure***

Lately method producing graphene sheets in atmospheric pressure microwave reactor by decomposition of ethanol was published [27]. This method produced graphene sheet in the gas phase without need of substrate with the same quality as methods like micromechanical cleaving or graphite oxide reduction. Graphene sheets were synthesized by passing liquid ethanol droplets into an argon plasma. The graphene sheets were characterized by transmission electron microscopy, electron energy loss spectroscopy, Raman spectroscopy, and electron diffraction.

### ***Acknowledgement***

We would like to thank M. Kadlečiková from Slovak Technical University Bratislava for Raman spectroscopy measurements, J. Buršík from Institute of Physics of Materials, ASCR Brno for SEM and TEM analysis and the team of Institute of Scientific Instruments, ASCR, Brno for HRSEM analysis. This work was supported by the Czech Ministry of Education under the projects MSM 0021622411 and by the Grant Agency of the Czech Republic contracts P205/10/1374, 202/08/0178, and 104/09/H080 and by the Academy of Sciences of the Czech Republic, contract KAN311610701.

### ***References***

- [1] H.W.Kroto, J.R. Heath, S.C. O'Brien, R.F. Curl, R.E. Smalley, *Nature*, 318, 1985, 162.
- [2] S.Iijima, *Nature*, 354, 1991, 56.
- [3] A.K.Geim and K.S. Novoselov, *Nature Materials*, 6, 2007, 183.
- [4] A. Thess, R. Lee, P. Nikolaev et.al., *Science*, 273,1996, 483.
- [5] M. Meyyappan, L. Delzeit, A. Cassell et.al., *Plasma Sources Sci. Technol.*, 2003, 12, 205.
- [6] M. Meyyappan, *J. Phys. D: Appl. Phys.*, 42, 2009, 213001.
- [7] Y. Li, W. Kim, Y. Zhang, M. Rolandi, D. Wang, H. Dai, *J. Phys.Chem.*, 105, 2001, 11424.
- [8] S. Hofmann, M. Cantoro, B. Kleinsorge et al.: *J. Appl. Phys.*, 98, 2005, 034308.
- [9] H. Takikawa, M. Ikeda, K. Hirahara et al., *Physica B: Condensed Matter*, 323, 2002, 277.
- [10] O. Smiljanic, B. Stansfield, J.-P. Dodelet et al., *Chem. Phys. Lett.*, 356, 2002, 189.
- [11] O. Jašek, M. Eliáš, L. Zajíčková et al., *Materials Science and Eng. C*, 26, 2006, 1189.
- [12] L. Zajíčková, M. Eliáš, O. Jašek et.al., *Plasma Phys. Control. Fusion*, 47, 2005, B655.
- [13] Y.-H. Lee, S.-H. Kyung, C.-W. Kim, G.-Y. Yeom, *Carbon*, 44, 2006, 799.
- [14] S.-J. Kyung, Y.-H. Lee, C.-W. Kim, J.-H. Lee, G.-Y. Yeom, *Carbon*, 44, 2006, 1530.
- [15] T. Nozaki, K. Okazaki, *Plasma Processes and Polymers*, 5, 2008, 300.
- [16] S. Esconjauregui, C.M. Whelan, K. Maex, *Nanotechnology*, 18, 2007, 015602.
- [17] M. S. Kabir, R.E. Morjan, O. A. Nerushev et.al., *Nanotechnology*, 16, 2005, 458.
- [18] E. Jiran, C.V. Thompson, *Thin Solid Films*, 208, 1992, 23.
- [19] J. Wen, J.W. Evans, M.C. Bartelt et.al., *Phys. Rev. Lett.*, 76(4), 1996, 652.
- [20] S. Pisana, M. Cantoro, A. Parvez et.al., *Physica E*, 37, 2007,1.
- [21] M. Cantoro, S. Hofmann, S. Pisana et.al., *Diam. Relat.Mater.*, 15(4-8), 2006, 1029.
- [22] H. Liu, G. Cheng, Y. Zhao et.al., *Surface and Coatings Technology*, 201(3-4), 2006,938.
- [23] M. Cantoro, S. Hofmann, S. Pisana et.al., *Nano Letters*,6, 2006, 1107.
- [24] W.H. Chiang and R. M. Sankaran, *Nature Materials*, 8, 2009, 882.
- [25] A. R. Harutyunyan, G. Chen, T. M. Paronyan et al., *Science*, 326, 2009, 116.
- [26] K. Hata, D. Futaba, K. Mizuno et.al., *Science*, 306, 2004, 1362.
- [27] A. Dato, V. Radmilovic, Z. Lee et al., *Nano Letters*, 8(7), 2008, 2012.

# COMPOSITE MATERIALS REINFORCED BY SHORT (NANO) FIBRES – COMPUTATIONAL SIMULATIONS

*Vladimír Kompis<sup>1</sup>, Miloš Očkay<sup>2</sup>, Peter Droppa<sup>2</sup>*

<sup>1</sup>*DSSI, a.s., Wolkrova 4, 85101 Bratislava, Slovakia*

<sup>2</sup>*Academy of Armed Forces, Demänovská 393, 03119 Lipt. Mikuláš, Slovakia*

Corresponding author: Vladimír.Kompis@aos.sk

**Abstract.** Composites reinforced by short fibres/tubes are often defined to be materials of future with excellent electro-thermo-mechanical (ETM) properties. The aspect ratio (length to diameter) of the short fibres is often  $10^3:1-10^6:1$ , or even more. Because of these properties very large gradients are localized in all ETM fields along the fibres and in the matrix. These fields define the interaction of the fibres with the matrix, with the other fibres and with the boundaries of the domain/structure. Method of Continuous Source Functions (MCSF) was developed by authors [1, 2] to simulate the interaction. Although the Carbon Nano-Tubes (CNT) have diameter of several nano-meters, their length is much larger and so, methods of continuum mechanics can be used also for the simulation of CNT with the matrix material. Main aim of our paper is to show some results of computational simulation for the interaction of fibres with the matrix and their contribution to increase stiffness, conductivity, strength and other properties of the composite material in micro- and macro-dimensions.

## Computational simulations and results

In the MCSF the interaction of matrix with fibres is solved as homogeneous continuum with material matrix properties and with 1D continuous source functions placed along fibre axes to simulate the continuity conditions in discrete points along the fibre/matrix boundaries (Fig. 1). The source functions are unit forces, dipoles and couples in statics. The force is vector function and the dipoles and couples are tensors obtained from the force as corresponding derivatives. The dipole is derivative of the force in the force direction and the couple in perpendicular direction to the force. In thermal problems the basic source is a unit heat source, i.e. it is scalar function and heat dipoles are derivatives of the heat source in corresponding direction, i.e. it is a vector function.

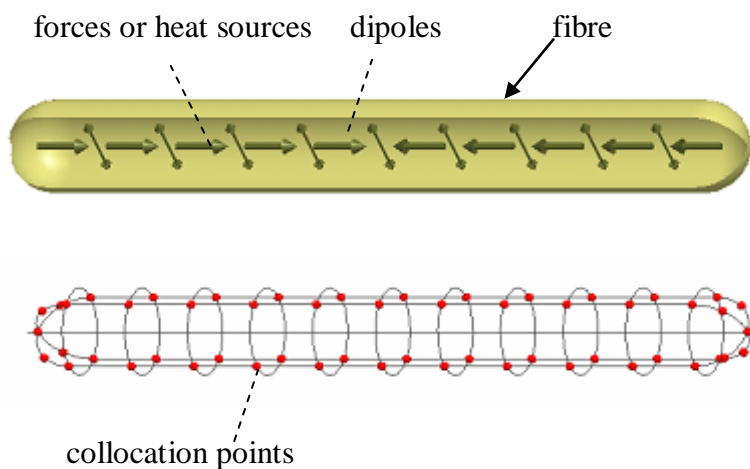


Fig. 1 Distribution of source functions and collocation points



It is supposed that the fibres have much higher stiffness, strength and conductivity than the matrix. Because of large aspect ratio also bending stiffness of fibres is negligible comparing to its axial stiffness. The micro-dimensions of the structure allow using multi-scale simulations in which the material properties are executed on micro-models and then they are homogenized for macro-model. Following continuity conditions are introduced between the fibre and the matrix:

In mechanics displacements are supposed to be constant in each fibre in the first iteration step. Moreover, because of the interaction between fibres, it is also necessary to prescribe displacements and strains to be equal in opposite points in cross-sections. The source functions located inside the fibre define resulting force acting in each cross section and from it one can obtain stresses and strains along the fibre, which can be used for corrections taking into account finite stiffness of the fibre in the next iteration steps.

Similarly constant temperatures are assumed in each fibre in the first iteration step and also additionally equal temperatures are prescribed on opposite sides of fibre cross-sections. The source functions inside fibres define in this case the heat flow in the fibre and taking into account its final conductivity, the continuity conditions are corrected in the next iteration steps.

Rigid body displacements of fibres and temperature changes by the interaction of fibres and matrix are obtained by satisfaction of force equilibrium and thermal energy conservation by source functions in each fibre.

Largest gradients in all potential fields are in the end parts of fibres. Their contribution to the interaction with the matrix is strongest. In mechanical problems, it is introduced by shear stresses and in thermal problems by the heat flow through the fibre/matrix interface (Fig. 2).

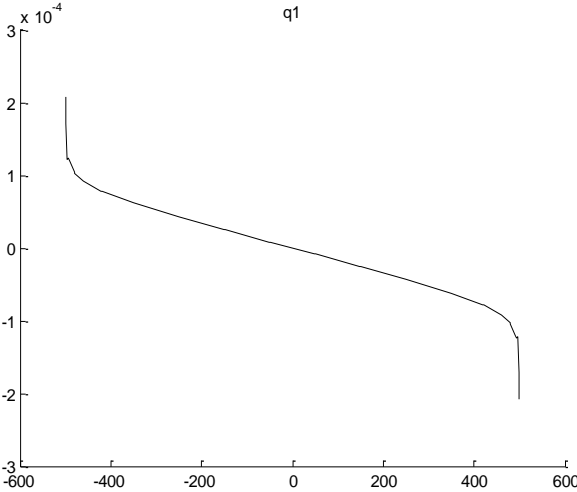


Fig. 2 Heat flow through the fibre surface along the fibre axis on single fibre in matrix material (L=1000R)

There is, however, also very strong interaction between neighbour fibres. Most important contribution to this interaction is close to the ends of closest fibres (see Fig. 3).

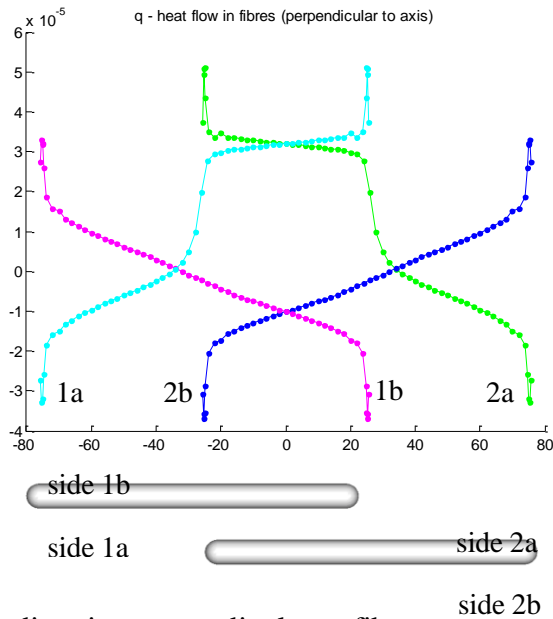


Fig. 3 Heat flow in direction perpendicular to fibres axes considering interaction

In a Control Volume Element (CVE) we have many fibres interacting together. Computational model has to take into account all these interactions in order to evaluate correctly mechanical and thermal properties of the composite material. Increase/decrease of temperature of fibres in a CVE of randomly distributed fibres is given in the Fig. 4. The CVE is in thermal field which correspond to the field of homogeneous material of the matrix with temperatures equal to corresponding coordinates in fibre axis direction. Diameter of fibres is equal to 2 and their length 200. Fibres which would intersect with other fibre, or are very close to another fibre are excluded from the computational model and so, there is no increment of the temperature in corresponding fibres in the Figure 4.

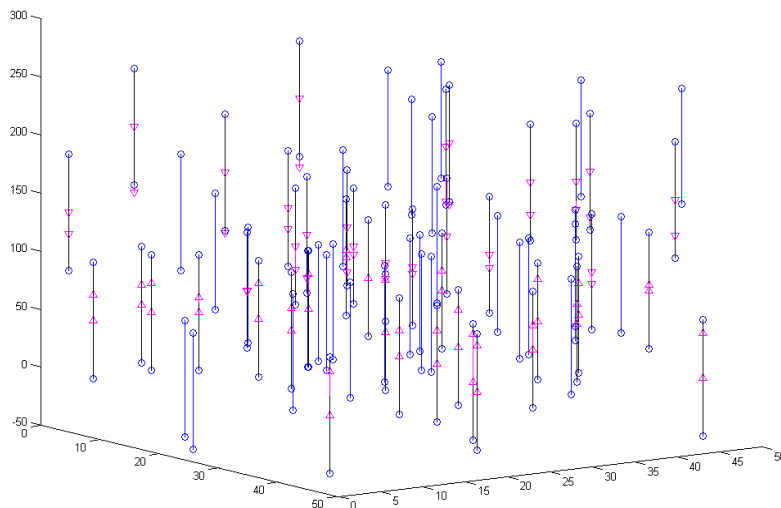


Fig. 4 Temperatures in patch of randomly distributed fibres

Behaviour of all mechanical, thermal, or electro-magnetic fields is similar, however, as the basic field variable in thermal field is scalar valued temperature, in mechanical field the displacement is vector having three components in 3D space, there are also three times more equations to be solved after the numerical discretization of the problem.

If the fibres are curved similar numerical procedure can be used as numerical evaluation is used in our models.

CNT are able to decohere and recohase in the end parts of fibres/tubes in the end parts, where there are very large shear stresses (Fig. 5). The region of very large shear stresses is usually very small and the decohesion/recohesion does not influence force transmission in other parts of fibres very much. The recohesion and recohesion is introduced by transmission of work from mechanical to thermal form and in dynamics by damping effect which is very important for some applications (turbine blades for aerospace engine, etc.).

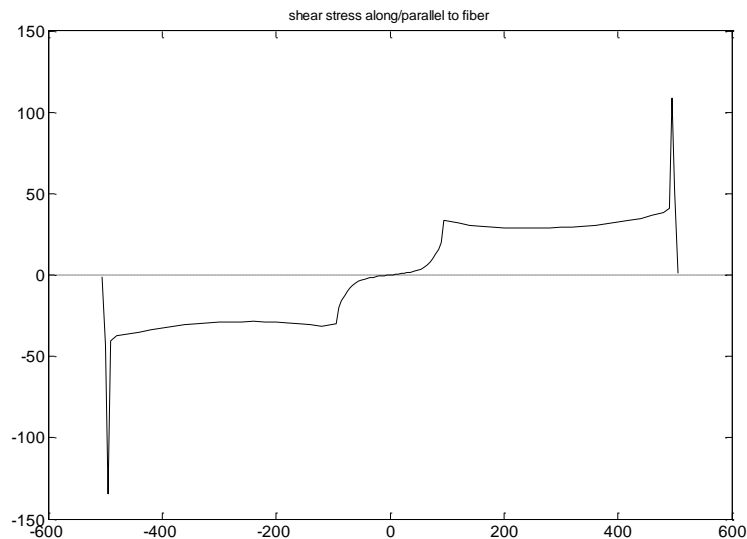


Fig. 5 Shear forces along fibre boundary (overlapping with neighbour fibres)

### Acknowledgement

Authors thank for NATO grant SVK-AVT-08\_1 and DSSI, a.s. for supporting this research.

### References

- [1] Method of continuous source functions for modeling of matrix reinforced by finite fibres, V. Kompiš, M. Štiavnický, M. Kompiš, Z. Murčinková, Q.-H. Qin, in V. Kompiš, ed. Composites with micro- and nanostructure, Springer, Dordrecht, 2008.
- [2] Temperature fields in short fibre composites, V. Kompiš, Z. Murčinková, M. Očkay, in Computational modelling and advanced simulations, to be published by Springer.

# ROLE OF THE SLOVAK CENTRE OF SCIENTIFIC AND TECHNICAL INFORMATION IN THE SUPPORT OF RESEARCH, DEVELOPMENT, INNOVATION AND TECHNOLOGY TRANSFER

*prof. RNDr. Ján TURŇA, CSc., Ing. Lubomír BILSKÝ*

*Slovak Centre of Scientific and Technical Information, Lamačská cesta 8/A, 811 04  
Bratislava, Slovak Republic*

Corresponding author: [turna@cvtisr.sk](mailto:turna@cvtisr.sk)

**The Slovak Centre of Scientific and Technical Information – SCSTI** (<http://www.cvtisr.sk>) is the national information centre and specialized scientific library of the Slovak Republic focused on all branches of technology and selected areas of natural and economic sciences. It is the state-owned institution with task to gather, process and provide science-related information and build complex information systems for research and development (R&D). The institution was established in 1938, while the most of the time in its more than **70-year history** was known as the Slovak Technical Library, which always belonged to pioneers in the process of new library technologies' implementation. The change of the name to the Slovak Centre of Scientific and Technical Information in 1996 should have meant also the extension of standard library services to other activities; however, the full development of non-library services has actually started only since 2007. Currently, the Slovak Centre of Scientific and Technical Information is the directly-managed organisation of the **Ministry of Education of the Slovak Republic**. It provides a wide range of library services including online catalogues, presence and absence loan services, etc. Besides that, the SCSTI offers also the possibility to loan books from other Slovak and foreign libraries, through the interlibrary loan services. In order to enable the easier and efficient orientation of users searching the information resources on the Internet, the specialised **SciTech navigator** has been developed, which contains the information about free accessible resources and systems on the Internet. For the benefit of library community, apart from educational activities, the Centre publishes specialized expert publications and the periodical “**ItLib-information technologies and libraries**”, as well as administrates the Internet portal **InfoLib**, which is focused on area of libraries and information science. Based on mutual agreements, the SCSTI hosts **depository libraries of the EU, the OECD and the EBRD**, the **Centre of Patent Information – PatLib** of the European Patent Office, as well as the **Sales Office of the EU Publisher** – Publications Office of the EU. The SCSTI builds and operates also the **EURO:i:portal** focusing on the issue of European integration.

## **New tasks of the SCSTI**

### **NCP SaT – National Centre for Popularisation of Science and Technology in Society**

In 2007, a new department called the **National Centre for Popularisation of Science and Technology in Society (NCP SaT)** has been created by the Ministry of Education of the SR within the SCSTI, with the aim to fulfil the tasks related to implementation of the Strategy of science and technology popularisation in society, which was approved by the government of

the Slovak Republic in February 2007. The mission of the NCP SaT is to raise wider public awareness of science, technologies and research results, while targeting mainly on the young generation; to promote the work of scientists and attract young people for studies at universities with orientation on technical and natural sciences. The NCP SaT attempts to initiate and create a forum for discussions among researchers about the achieved R&D results and the importance of active participation of the Slovak R&D organisations in international science and technical co-operation. Following this objective, the NCP SaT organises a number of events on a regular basis. The most important and popular ones are: “Science in the centre” – a cycle of science cafes meaning the informal meetings of scientists with experts and wider public in the SCSTI premises; “Scientific confectioners” – co-organised with the so called Young Slovak Researchers Association aimed at involving the elementary and secondary school students and their teachers in a relaxed way in the scientific discussions with well-known scientists; and “The week of science and technology in Slovakia” – where the SCSTI supports the Ministry of Education of the SR in organisation of main and accompanying events, conferences and competitions. In addition to these activities, the NCP SaT organises continuously lectures at schools, as well as exhibitions focused on science promotion.

The SCSTI has also been authorised by the Ministry of Education of the SR to ensure the operation of the **Central information portal for research, development and innovation (CIP RDI)**, which is one of the main information, managerial and supervisory tools of the state scientific and technical policy. CIP RDI provides information related to the state support of science, financing, relevant official documents, selected statistical data, implementation of European regulations, international science co-operation, R&D results, public calls for research projects, as well as records of all research, development and innovation projects and tasks financed partially or in total from public sources, together with the evaluation of their socio-economic outcomes. The portal contains the following data since the year 2000:

- Calls for proposals for research related projects;
- More than 600 organisations from area of science and research;
- Database of more than 4.000 implemented research projects;
- Database of more than 1.000 experts from various science fields;
- Characteristic of more than 3.000 laboratories and research facilities.

Furthermore, the CIP RDI serves as a tool for the:

- Effective organization and implementation of the agenda called “Science and Society” in Slovakia;
- Valuation of state and regional potential in area of research, development and innovation;
- Follow-up the effectiveness of public funds provided for R&D support.

Currently, the CIP RDI is being augmented with new functions, mainly in terms of effective handling with projects throughout their life-cycle and interconnection with other R&D related information systems. Moreover, the improvement of English version of the portal will be finished soon and thus the portal will become an effective support tool also for foreign

researchers, entrepreneurs and venture investors interested in the Slovak R&D. The portal can be visited at the following link: <https://www.vedatechnika.sk>



**The SCSTI national projects financed from the EU structural funds, Operational programme Research and development**



### **National information system promoting research and development in Slovakia – Access to electronic information resources – NISPEZ**

The access to electronic information resources (EIR) is the basic prerequisite for the knowledge-based society development. Until 2008, the research and scientific community in Slovakia accessed the electronic information resources (EIR) through academic libraries at individual universities, which had to submit each year the development projects to the Ministry of Education of the SR in order to obtain means for subscriptions. The Slovak Academy of Sciences obtained and paid for licensed EIR for its researchers from its own budget line. By the end of 2008, the SCSTI started an implementation of the national project called NISPEZ, which is financed from the EU structural funds – European Regional Development Fund (ERDF), Operational programme Research and development. The main objective of the project is to ensure the access to electronic information resources in the field of research and development for the science community and university students in Slovakia. The end of the project is planned for June 2014 and the total amount of grant provided is 19.881.676,23 EUR. In this long-term period of 5 years, it will handle the co-ordinated purchase and access provision to EIR for research and development in Slovakia, creation of the database of Slovak EIR and also augmenting of CIP RDI with new functions focused on interconnection with other information systems on research and development, while respecting the EU standards, especially data model CERIF (Common European Research Information Format). Within the NISPEZ project, the access (for academic and research community in Slovakia) to the following databases is being provided: **ACM / Association for Computing Machinery; Art Museum Image Gallery; Gale Virtual Reference Library: Art; IEEE/IET Electronic Library (IEL); Knovel Library; ProQuest Central; REAXYS; (originally Beilstein-CrossFire Direct); ScienceDirect; SCOPUS; SpringerLink; Web of Knowledge; and Wiley InterScience.**

### **Data centre for research and development – DC-R&D**

The SCSTI currently implements another national project within the Operational programme Research and development (ERDF) called “Infrastructure for Research and Development – the Data centre for research and development”. The main project objective is to build a data centre, which will store, process and provide access to information that is needed by Slovak scientific organisations while carrying out their R&D activities. Within the project, progressive ICT infrastructure for research and development area will be built, with purpose to store and provide data used by researchers, while ensuring a high level of accessibility and security. At the same time, the infrastructure for electronic communication in area of science and research will be created. The total amount of grant provided from EU structural funds for this project implemented in period 2009 – 2014 is 33.133.963,58 EUR.

## **The SCSTI and the technology transfer support**

During 2009, there are first offices focused on technology transfer support being established at Slovak universities and research institutions. However, since the **technology transfer (TT)** is a relatively new issue in Slovak conditions (similarly as in other eastern-European countries), there is an obvious need for assuring the co-ordination of activities of individual centres, support their development and thus create an effective system for TT support at national level. The key part of the system should, according to the decision of the Ministry of Education of the SR, be the Slovak Centre of Scientific and Technical Information together with local TT centres established at universities and R&D organisations. With regard to this new task, the SCSTI has established a Technology transfer department, which will be further developed and transformed mainly within another EU structural funds' project implemented by the SCSTI.

The SCSTI has recently finished the preparation of the above-mentioned national project called "**National infrastructure for technology transfer support in Slovakia – NITT SK**", which has been submitted to the programme's Managing authority. The project beginning is planned for June 2010, while the implementation should be finished in December 2014; nevertheless, the SCSTI has the ambition to continue with TT support activities also after the project termination. Again, the project will be financed from the EU structural funds (ERDF) within the Operational programme Research and development. The planned total budget of the project is nearly 8,5 million EUR and the main objective is to create and implement the national support system for transferring the knowledge and technologies gained by R&D activities to socio-economic praxis, with the aim to contribute to knowledge-based economy development. The project intention is to propose and implement the national infrastructure for technology transfer support, and thus contribute directly to more intensive and efficient state support of research and development. The national system will support those R&D activities that reflect the real needs of entrepreneurial sector, which will result in increased application of R&D results and technologies in industry. At the same time, it will support the creation of long-term partnerships between academy and industry, which will help not only to academics themselves, but it will contribute to the sustainable development of the whole, knowledge-based society. The NITT SK project will be implemented nation-wide at the whole territory of the SR, while the primal target group of the project will be the science community coming from public sector. The project will be focused on achieving the following three specific objectives:

- Building-up the Technology transfer centre at the SCSTI, in order to ensure the systematic technology transfer support at national level;
- Support the science community in the process of technology transfer through utilisation of existing ICT capacities and resources for research and development;
- More efficient transfer of technologies and scientific knowledge to economy and society through the science promotion.

The SCSTI transformation towards progressive approaches in the field of access, organisation and provision of scientific information, as well as orientation on new tasks and support

services is a long-lasting process, which is significantly accelerated due to an effective use of means provided within the EU structural funds.



# PROPERTIES OF FE-CO NANOPOWDER PREPARED BY CHEMICAL SYNTHESIS

***K. Zábranský, O. Schneeweiss***

*Institute of Physics of Materials, AS CR, Brno, Czech Republic*

Corresponding author: zabransky@ipm.cz

**Abstract.** Chemical synthesis of binary Fe-Co oxalate was used for preparation Fe-Co nanoparticles. X-ray diffraction spectra recorded during temperature treatment in reduction atmosphere shows two main stage of transformation. The amorphization of oxalate mixture and formation of Fe-Co nanoparticles respectively. After X-ray diffraction high temperature treatment the nanoparticles with 50 nm mean crystalite size was found. Comparison of magnetic properties during and after different type of temperature treatment show us that coercivity and saturation magnetic polarization are sensitive in dependence on sample condition, length of treatment and temperature. Analysis of Mössbauer spectra reveal several components which were ascribed different phases evolving during temperature treatments.

## INTRODUCTION

Iron-cobalt nanoparticles are well known for their good magnetic properties. High value of magnetization, low coercivity and high Curie temperature create a potential for applications in medicine, high density recording media or as a catalyst [1-3]. Several method for preparation FeCo has been recently developed, e.g., chemical or physical vapor deposition, sol-gel technique, laser pyrolysis. Thermal decomposition of oxalates precursor was applied as well [4]. In our work the different procedure for preparation of binary Fe-Co oxalate was used. Creation solid state mixture by segregation from solution allows mixing of the different metal species on an atomic scale. In the case of materials containing more than one metal, this method also enables a good control over the relative proportions of the elements.

In this work we studied the process of synthesis the nanocrystalline phase in dependence on temperature treatment and properties of the prepared material.

## EXPERIMENTAL DETAILS

Binary solid state Fe-Co oxalate precursor was prepared by segregation from Fe and Co sulfate solution. The nanoparticles were prepared by thermal decomposition of binary Fe-Co oxalates in hydrogen atmosphere.

The phase analysis of the samples was carried out by X-ray diffraction (XRD) using  $\text{CoK}\alpha$  radiation. High temperature XRD measurements were done in Anton Paar TCU 2000 furnace with a platinum heating strip. The high temperature XRD measurement was used for the study of the formation of FeCo nanocrystalline phase. After the short scan ( $2\theta$  from  $38^\circ$  to  $66^\circ$  for 30 minutes) measurement at  $100^\circ\text{C}$  the temperature increased gradually to  $600^\circ\text{C}$  with the step  $\Delta T = 20^\circ\text{C}$  and for every step the short scan was taken. Finally the diffraction in the whole  $2\theta$  range was measured at room temperature. The sample was for the whole time under hydrogen atmosphere. For better determination of the beginning of precursor amorphization and formation of FeCo phase the measurement with the temperature steps  $\Delta T = 5^\circ\text{C}$  were taken in critical temperature region ( $150 \div 300^\circ\text{C}$ ).

Additional information on size morphology and structure was obtained using transmission electron microscopy.

Mössbauer spectroscopy (MS) was measured at room temperature and at several low temperatures. Spectra were taken in transmission geometry using the  $^{57}\text{Co}/\text{Rh}$  source and evaluated using CONFIT program package [5]. Velocity scale was calibrated with a standard thin  $\alpha$ -iron foil.

Fe-Co oxalate precursor was annealed in resistance furnace at 560 °C in hydrogen atmosphere for 2 hours.

Hysteresis loops were measured by vibrating sample magnetometer in magnetic field up to 796 kA/m. Thermomagnetic curves were taken at constant field 4kA/m in  $\text{H}_2$  atmosphere.

Temperature regime was 20  $\rightarrow$  800  $\rightarrow$  20 °C with the temperature sweep 4 °C/min. Before and after the thermomagnetic measurements hysteresis loops were measured.

## RESULTS AND DISCUSSION

X-ray diffraction patterns of the as-prepared precursor-sample confirm requested composition, respective Fe-Co oxalate. The recorded patterns show also traces of iron sulfate which indicate that impurities remained from the precursor preparation. In fig. 1 are shown selected high temperature XRD patterns. At 150 °C the amorphization of precursor which is first stage decomposition of Fe-Co oxalate was found. Solid solution  $\alpha$ -FeCo diffraction peaks appeared at 290 °C. The mean coherence length is increasing with rising temperature which is represented by peaks intensity and line widths. This is a consequence of ordering processes in FeCo phase. Using the Scherrer equation the mean coherence length was calculated and it is increasing from  $\sim$  30 nm at 290 °C to  $\sim$  90 nm in the end of the heat treatment. The XRD patterns of sample after temperature treatment and exposition to air atmosphere shows only FeCo phase without any traces of oxides. This good resistance against oxidation can be ascribed to the high content of cobalt in the nanopowder.

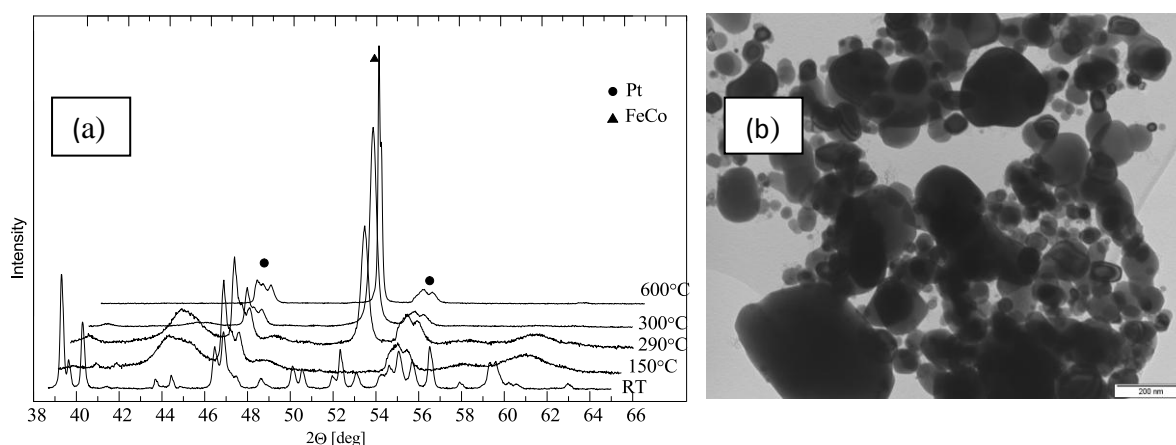


**FIGURE 1.** XRD patterns measured at different annealing temperatures (a), TEM image of the nanoparticles (b).

The image from transmission electron microscopy of the sample after the high temperature XRD measurement is shown on fig. 1 a. A broad size distribution (approximately 40  $\div$  200 nm) can be observed there. EDX analysis of selected particles proved that chemical composition Fe to Co is 50:50 with very low fluctuations. The point diffractions confirm bcc structure of the particles.

Thermomagnetic curve shown in Fig. 2 exhibits a rapid increase in temperature range 350-400 °C which is due to formation of FeCo ferromagnetic phase. The slow decrease above 400 °C is probably associated with magnetic hardening caused by grain growth and formation magnetocrystalline anisotropy. The fine increase with decreasing temperature is in agreement with the temperature dependences of magnetic moments of ferromagnetic materials. The

difference can be ascribed to different form of the samples. While for the thermomagnetic measurement a compacted (pressed) form of a small cylinder was used, the powder for XRD measurements was strewn on the heating Pt strip. An access of hydrogen to the particles was much easier in case of XRD measurement, and therefore the chemical reduction is easier there.

The parameters derived from the hysteresis loops taken after the different heat treatments are summarized in Table 1. The differences in all parameters can be ascribed to the grain size and free surface area of the particles during the heat treatment. Coercivity  $H_c$  is decreasing with the increasing of maximum temperature of the annealing, i.e. with grain size. On the contrary, saturation polarization  $J_s$  is increasing and it corresponds to the increasing ratio of atoms in grain interiors to grain surfaces.

**TABLE 1.** The parameters the hysteresis loops taken after the different heat treatments of the precursor in hydrogen atmosphere (coercivity,  $H_c$ , saturation polarization  $J_s$ , remanent polarization  $J_r$ ).

| Heat treatment                          | $H_c$ [kA/m] | $J_s$ [T] | $J_r$ [T] |
|---|--------------|-----------|-----------|
| After thermomagnetic curve up to 800 °C | 1.52         | 2.45      | 0.046     |
| After high temperature XRD up to 600 °C | 14.24        | 2.32      | 0.395     |
| After furnace annealing up to 560 °C    | 23.20        | 1.68      | 0.440     |

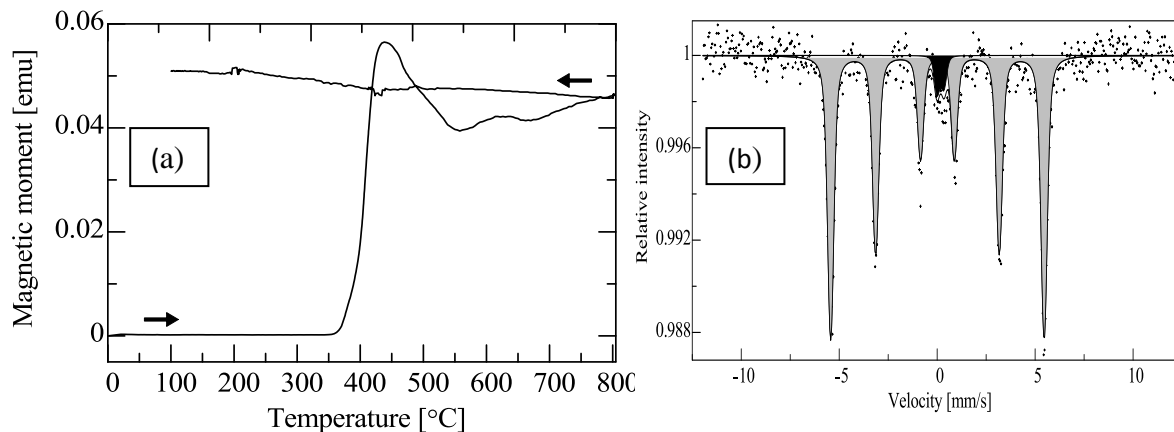


**FIGURE 2.** Thermomagnetic curve of the Fe-Co oxalate taken in hydrogen atmosphere, dynamic (a), Mössbauer spectrum of the sample after the measurement of the thermomagnetic curve. The sextet components are filled by diagonal cross and the doublet by black. (b).

Mössbauer spectrum of the sample which was treated during thermomagnetic curve measurement is drawn in Fig 2 b. Three components were used for good fit of the experimental data: (i) the sextet with the line width close the line width obtained for the sextet in the spectrum of iron in calibration sample, (ii) broad sextet described by distribution of hyperfine field, (iii) the doublet. The parameters of the components are given in Table 2. Mössbauer spectrum of the sample after high temperature XRD yielded the same results. The high value of hyperfine field of the first sextet implies that it represents FeCo nanoparticles. The second sextet described by the distribution of hyperfine field corresponds to iron atoms in surface regions of the nanoparticles and possible fluctuations in chemical composition. The doublet can be ascribed to superparamagnetic particles. According to [6] the superparamagnetic state is achieved for particles FeCo smaller than 34 nm. Furthermore, in the spectrum taken on the sample after the thermomagnetic curve measured to 560 °C only a higher atomic fraction of the doublet was analyzed.

**TABLE 2.** The hyperfine parameters of Mössbauer spectra: atomic fraction of iron atoms, A, hyperfine field  $B_{\text{hf}}$ , distribution of hyperfine field,  $\Delta B_{\text{hf}}$ , isomer shift,  $\delta$ , quadrupole shift  $\epsilon$ , quadrupole splitting,  $\Delta E_{\text{Q}}$ .

| Component | A [%] | $B_{\text{hf}}$ [T] | $\Delta B_{\text{hf}}$ [T] | $\delta$ [mm/s] | $\epsilon$ [mm/s] | $\Delta E_{\text{Q}}$ [mm/s] |
|-----------|-------|---------------------|----------------------------|-----------------|-------------------|------------------------------|
| 1. Sextet | 78±2  | 34.1±0.1            | -                          | 0.03±0.01       | 0,02±0.01         | -                            |
| 2. Sextet | 16±2  | 35.0±0.1            | 2.0±0.2                    | 0.02±0.01       | -0.93±0.02        | -                            |
| Doublet   | 6±1   | -                   | -                          | 0.14±0.01       | -                 | 0.49±0.01                    |

## CONCLUSION

We have shown that FeCo nanoparticles can be prepared by reduction of binary FeCo oxalate in hydrogen atmosphere. The chemical composition of the powder was close to the requested concentration Fe<sub>50</sub>Co<sub>50</sub>. XRD, Mössbauer spectroscopy and TEM results confirmed bcc structure of the particles. Comparison of the critical temperatures for decomposition of the precursor and formation of FeCo particles was obtained from temperature dependences of XRD diffractions and magnetic moment measurements. They indicate that the kinetics of the process is strongly influenced by the form of the sample. Similar large difference can be observed on the parameters of hysteresis loops taken after different methods of heat treatments.

## ACKNOWLEDGMENTS

This work was supported by the Ministry of Education, Youth and Sports of the Czech Republic (Project No. 1M6198959201) and by the Grant Agency of the Czech Republic (Project No. 106/08/1440).

## REFERENCES

1. A. Figuerola, R. Di Coratob, L. Manna, T. Pellegrino, *Pharmacol. Res.*, article in press (2010).
2. R. H. Kodama, *J. Magn. Magn. Mat.* **200**, 359-372 (1999).
3. P. Yuan, H. Wu, H. Xu, D. Xu, Y. Cao, X. Wen Wei, *Mater. Chem. Phys.*, **105**, 391-394 (2007).
4. H.S. Horwitz, J. M. Longo, *Mater. Res. Bull.*, **13**, 1359-1369 (1978).
5. T. Zak and Y. Jiraskova, *Surf. Interf. Anal.* **38**, 710-714 (2006).
6. S. Majteych, Y. Jin, *Science* **284**, 470 (1999).

# ZVIDITEĽNOVANIE KRYŠTALOGRAFICKÝCH DEFEKTOV V GaP POMOCOU MOKRÉHO CHEMICKÉHO LEPTANIA

***Božena Matušková\*, Jaroslava Škriniarová***

*Katedra mikroelektroniky, Fakulta elektrotechniky a informatiky,*

*Slovenská technická univerzita, Bratislava*

*\*E-mail: boba.matuskova@gmail.com*

Práca je zameraná na štúdium vzniku štruktúrnych porúch v polovodičových materiáloch skupiny III – V, následne ich vplyvmi, či už na kvalitu daného materiálu, alebo kvalitu súčiastky pre elektroniku a optoelektroniku z neho vyrobenej. Analyzovali sme materiály VGF GaP (100), LEC GaP (100) a LEC GaP (111)<sub>B</sub>. Na základe teoretických poznatkov týkajúcich sa odhaľovania kryštalografických porúch pomocou metódy mokrého chemického leptania boli vykonané experimenty. Výsledky boli zaznamenané optickým, atómovým silovým (AFM) a elektrónovým mikroskopom (SEM). Cieľom práce bolo zviditeľniť poruchy, ktorých rozmery sa pohybujú v škále od niekoľkých nanometrov až po niekoľko desiatok mikrometrov, ako aj identifikovať pravepodobný pôvod ich vzniku. V závere práce je diskusia zameraná na odhalené poruchy v mriežke VGF GaP, LEC GaP (100) a LEC GaP (111)<sub>B</sub>.

## ÚVOD

GaP je jedným z veľmi často používaných polovodičových materiálov na výrobu svetlo emitujúcich diód (LED) pre spektrum viditeľného žiarenia. Podmienkou pri výrobe elektronických a optoelektronických súčiastok je hlavne kvalita materiálu, z ktorého sú vyrobené. Dôvodom je vplyv kvality daného materiálu na elektrické a optické vlastnosti súčiastok. Preto by sa mala upriamiť značná pozornosť hlavne na štruktúrne poruchy polovodičových materiálov. Posúdenie kvality materiálu môže byť uskutočnené rôznymi metódami analýzy látok. Rýchlym, lacným a jednoduchým spôsobom posúdenia kvality materiálu je zviditeľňovanie kryštalografických porúch pomocou mokrého chemického leptania. Chemické leptanie je jedným z veľmi dôležitých procesov pre štúdium kvality GaP. Na detekciu dislokácií sa v kryštáli GaP môžu použiť rôzne leptadlá. Pri experimentoch sme sa opierali o poznatky získané z vedeckých článkov. V. Gottschalch et al. popisuje vo svojom článku [1] použitie H<sub>3</sub>PO<sub>4</sub>, ako aj vplyv materiálu a podmienok leptania na tvar odleptaných jamiek. M. Umeno a H. Kawabe [2] uvádzajú použitie leptadla RC, kedy leptaním zviditeľnili dislokácie. Názov RC leptadla pochádza z iniciálok jeho objaviteľov J. L. Richardsa a A. J. Crockera (1960). Robert H. Saul [3] rozoberá v článku štyri rôzne leptadlá a ich vplyv na jednotlivé strany materiálu, kedy leptadlo odhaľuje na určitej strane (napr. gáliovej) materiálu defekty, pričom na strane druhej (fosforovej) sa používa na leštenie. Ďalej uvádza aj použitie leptadla AB (iniciály objaviteľov Abrahams a Buiocchi, 1965), ktorým zviditeľnil dislokácie a vrstevné chyby na oboch stranách materiálu.

## POUŽITÝ MATERIÁL A EXPERIMENTÁLNE POSTUPY

Skúmali sme GaP vyrobený metódou Liquid Encapsulated Czochralski (LEC) narezaný v rovinách (100) a (111) a Vertical Gradient Freeze (VGF) narezaný v rovine (100). Pri mokrom chemickom leptaní boli použité nasledovné leptadlá:

**H<sub>3</sub>PO<sub>4</sub>** (85%)

**H<sub>2</sub>SO<sub>4</sub>** (94%)

**AB leptadlo** (10ml H<sub>2</sub>O : 40mg AgNO<sub>3</sub> : 5gCrO<sub>3</sub> : 8ml HF)

**RC leptadlo** (8 ml deionizovanej  $H_2O$  : 10 mg  $AgNO_3$  : 6 ml  $HNO_3$  : 4 ml HF)  
Odleptané vzorky sme analyzovali pomocou optického interferenčného mikroskopu, ktoré sme mali možnosť zaznamenať digitálnou kamerou. Navyše boli vzorky analyzované AFM Park XE – 100, SEM LEO 1550. Profily vzoriek boli vyhodnocované pomocou Dektaku na KME.

## DOSIAHNUTÉ VÝSLEDKY A DISKUSIA

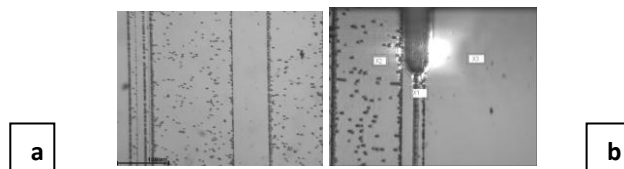
Prítomné kryštalografické poruchy v materiáli sme zviditeľnili metódou mokrého chemického leptania použitím rôznych leptadiel. Špecifikovali sme ich a uviedli sme možné príčiny ich vzniku. Materiál VGF GaP (100) sme skúmali v dvoch oblastiach, a to na okraji a v strede substrátu. Ďalej sme v našich experimentoch skúmali materiál vyrobený LEC metódou roviny (100), ako aj (111)<sub>B</sub>.

### 1. OKRAJ SUBSTRÁTU VGF GaP

Prítomnosť vrstevných porúch a odleptaných jamiek sme detekovali na vzorke odobranej z okraja doštičky VGF GaP. Ich vznik je daný nesprávnymi podmienkami v procese chladnutia kryštálu.

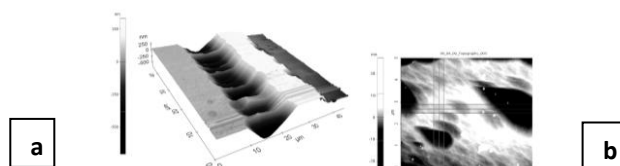
#### $H_3PO_4$

Koncentrovanú kyselinu fosforečnú sme zahriali na  $185^\circ C$  a leptali sme ňou po dobu 4 minút. Stanovením týchto podmienok leptania sme odhalili na vzorkách z okraja doštičky VGF GaP poruchy kryštalickej mriežky, ktoré zodpovedajú dislokáciám, vrstevným chybám (sklz) a dvojčateniu.

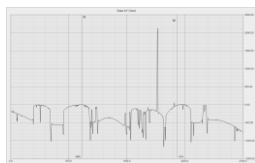


Obr. 1 VGF GaP a) po leptaní v  $H_3PO_4$ , 4min,  $185^\circ C$ , b) oblasť skenu vzorky pomocou AFM

Pomocou AFM sme analyzovali povrch oblasti s vysokým počtom dislokácií, ako aj oblasti s nižším počtom defektov (obr. 1b). Jednotlivé oblasti sú označené ako X1, X2 a X3.



Obr. 2 Profil oblasti a) X1, hĺbka odleptanej dislokačnej čiary je približne 500 nm, b) X2 (viac defektnej)



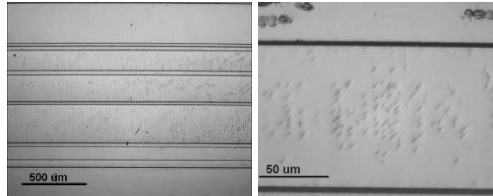
Obr. 3 profil vzorky z okraja doštičky VGF GaP po leptaní v  $H_3PO_4$ , 4 min

Tieto zviditeľnené poruchy sme priradili k plošným poruchám, konkrétne vrstevným chybám – sklzu rovín a zrkadlovému zrastu rovín kryštálov – dvojčatenie. Plošné poruchy vznikajú pravdepodobne pri procese chladenia kryštálu. Existenciu plošných porúch sme dokázali pomocou merania profilu Dektakom (obr. 3). Na základe týchto meraní sme zistili rôzne rýchlosti leptania na susedných častiach plochy vzorky oddelených dislokačnou čiarou. V prítomnosti jednej roviny (napr. (100)), rýchlosť leptania by bola rovnaká. Medzi dvomi plochami oddelenými dislokačnou čiarou by nebol výškový

rozdiel. V prípade, že jedna rovina sa leptá rýchlejšie ako druhá, dochádza pravdepodobne k zrkadleniu dvoch rovín – dvojčateniu. Na povrchu vzorky VGF GaP predpokladáme prítomnosť rovín (100) a (111).

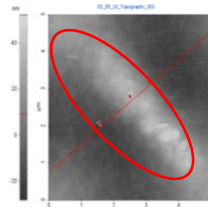
### AB leptadlo

Zloženie AB leptadla je podobné zlúčenine RC leptadla. Leptadlo sme zahriali na 70°C - 80°C. Leptaním po dobu 25 minút sme dokázali takisto prítomnosť plošných porúch (obr. 4) na okraji doštičky VGF GaP.



**Obr. 4** zviditeľnené plošné poruchy na okraji VGF GaP leptanom v AB, 70°C - 80°C, 25min

Na obr. 5 je detail čiarovej poruchy pomocou AFM. Výška čiarovej poruchy je približne 58 nm.

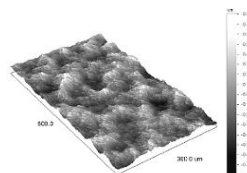


**Obr. 5** detail čiarovej poruchy pomocou AFM na okraji VGF GaP leptanom v AB, 70°C - 80°C, 25min

## 2. STRED SUBSTRÁTU VGF GaP

### RC leptadlo

Povrch stredu substrátu VGF GaP po dobe leptania 30 minút zahriatym RC leptadlom zostáva veľmi drsný. Prítomnosť dislokácií ani iných porúch sme nezaznamenali (obr. 6).

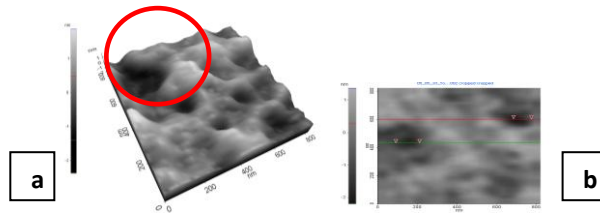


**Obr. 6** povrch stredu substrátu VGF GaP po leptaní v RC leptadle pomocou Dektaku

## 3. LEC GaP (100)

### H<sub>3</sub>PO<sub>4</sub>

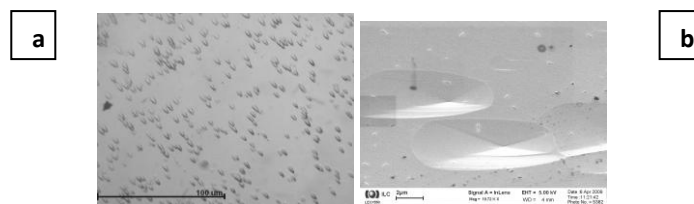
Prítomnosť dislokácií sme detekovali na vzorke LEC GaP. Ich vznik je daný procesom rastu kryštálu. Už po leptaní 35 sekúnd v zahriatej kyseline fosforečnej na 160°C sa zviditeľnia nanorozmerné dislokácie (obr. 7, obr. 8), ktoré potom zviditeľňujeme do rozmerov viditeľných okom, aby sme boli schopní vyhodnotiť ich hustotu na určitú plochu.



**Obr. 7 a) AFM záznam nanorozmernej dislokácie, b) AFM analýza: priemer dislokácie je približne 119 nm, hĺbka sa pohybuje v rozmedzí 0,5 – 1,5 nm**

Leptaním po dobu 4 minút zahriatou kyselinou fosforečnou na 185°C sme zviditeľnili dislokácie do rozmerov, ktoré sú vyhovujúce pre vyhodnotenie z hľadiska hustoty odleptaných jamiek.

Hustota odleptaných jamiek (EPD, angl. Etch Pits Density) je  $3,34 \cdot 10^5 \text{ cm}^{-2}$  (údaj sa zhoduje s údajom udávaným výrobcom).



**Obr. 85 a) Dislokácie v LEC GaP, leptanom v  $\text{H}_3\text{PO}_4$ , 4 min, 185°C, b) Detail dislokácií v LEC GaP pomocou SEM**

Na obr. 8 b) si môžete všimnúť špecifický tvar dislokácie zodpovedajúci kubickej mriežke, roviny (100).

### **AB leptadlo**

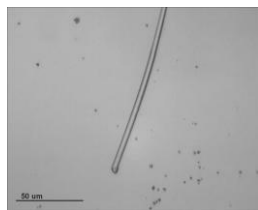
Materiál vyrobený Czochralského metódou sme ďalej leptali zahriatym AB leptadlom na 70°C - 80°C po dobu 20 minút.

Výsledkom boli dislokácie, ktoré sa zhľukujú do čiar. Pravdepodobne vznikajú pri nesprávnych podmienkach rastu kryštálu.

## **4. LEC GaP (111)**

### **AB leptadlo**

Zlúčenina AB leptadla zviditeľnila na materiáli LEC GaP roviny (111) dislokácie a časti dislokačných slučiek (obr. 9) po leptaní 15 minút a zahriatí na 70°C - 80°C.

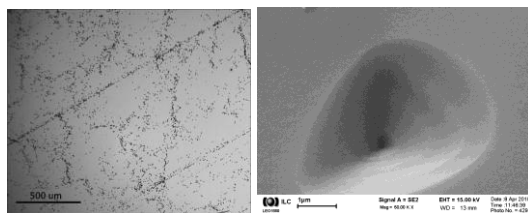


**Obr. 9 dislokácie a časti dislokačných slučiek po leptaní 15 min, 70°C - 80°C.**

### **RC leptadlo**

Zlúčenina RC leptadla nám po leptacom procese (70°C - 80°C, 1 minúta) zviditeľnila dislokácie a zhľuky čiarových porúch (obr.10).





**Obr. 10** dislokácie po leptaní v RC leptadle, 70°C - 80°C, 1 min

Hustota odleptaných jamiek (EPD) je  $6.10^7/\text{cm}^2$ , čo je až o dva rády viac ako hustota odleptaných jamiek v materiáli LEC GaP roviny (100). Môžeme konštatovať, že sa jedná o menej kvalitný materiál

## 5. ZÁVER

V príspevku sme sa venovali štúdiu a porovnaniu štruktúrnych porúch v materiáli LEC GaP a VGF GaP. V mriežke LEC GaP sa nám zviditeľnili štruktúrne čiarové poruchy, tzv. dislokácie. Príčinou ich vzniku môžu byť nesprávne podmienky rastu kryštálu. Prítomnosť plošných porúch, konkrétne vrstevných chýb – sklz rovín a zrkadlový zrast kryštálov – dvojčatenie sme zaznamenali v mriežke materiálu VGF GaP odobraného z okraja substrátu. Vznik týchto porúch môžeme pravdepodobne prisúdiť nevhodným podmienkam chladnutia pri raste kryštálu. Naopak materiál VGF GaP odobraný zo stredu substrátu vykazuje vysokú čistotu.

## PodĎakovanie

Chceli by sme sa poďakovať za merania RTG topografiou, odborné rady a konzultácie Doc. RNDr. Edmundovi Dobročkovi, CSc. (ELÚ SAV). Za merania profilov Dektakom ďakujeme Ing. Ivanovi Novotnému, PhD., Bc. Tomášovi Ščepkovi ďakujeme za AFM analýzy (KME). Táto práca bola urobená s podporou Centra Excelencie CENAMOST (Slovak Research and development Agency Contract No. VVCE-0049-07) s podporou grantu VEGA 01/0689/09.

## 6. Použitá literatúra

- [3] GOTTSCHALCH V., et al.:  $H_3PO_4$  – Etching of (001) – Faces of InP, (GaIn)P, GaP, and Ga(AsP), in *Kristall und Technik*, 1979, s. 569 – 569
- [4] Umeno, M., Kawabe, H.: HVEM investigations of crystal defects in S doped LEC GaP crystals, *Philosophical Magazine A*, 1979, Vol. 39, No. 2, 183 – 194
- [5] SAUL, R.: The defect structure of GaP Crystals grown from gallium solutions, vapour phase and liquid phase epitaxial, *J. Electrochem. Soc.: Solid state science, Defect structure of GaP crystals*, vol. 115, no. 11, s. 1184 - 1190
- [6] IZUKA, T.: Etching studies of Impurity Precipitates in pulled GaP Crystals, *J. Electrochem. Soc.: Solid state science, Etching study of pulled GaP crystals*, vol. 118, no.7, s. 1190 - 1194
- [7] LAISTER, D., JENKINS, G.M.: Dislocations and Twins in LEC grown GaP Single Crystals, *Journal of materials science* 5, 1970, s. 862 - 868

# POINT OF CARE TESTING ( POCT ), NANOTECHNOLÓGIE A PERSONALIZOVANÁ LABORATÓRNA DIAGNOSTIKA

***Gustáv Kováč, Pavel Blažíček***

*Ústav chémie, klinickej biochémie a laboratórnej medicíny, Slovenská zdravotnícka  
univerzita, Inštitút laboratórnej medicíny Alphamedical as  
gustav.kovac@alphamedical.sk*

## **Úvod**

Za posledných 20 rokov prišlo v laboratórnej diagnostike k

- narastaniu spektra a objemu laboratórných vyšetrení
- zvyšovaniu pracovnej záťaže laborantov
- skracovaniu TAT ( turn around time )
- rastu požiadaviek na kvalitu
- akreditáciám klinických laboratórií
- rozpočtovým obmedzeniam.

Odpoveďou na tento vývoje bola

- automatizácia a konsolidácia laboratórnej diagnostiky -vo vnútri laboratórií
- fúzie laboratórií s rozličnými špecializáciami ( hematológia, biochémia, mikrobiológia, imunológia ), koncentrácia laboratórií a outsourcing laboratórných aktivít nemocnicami – na medzilaboratórnej úrovni
- využívanie nanotechnológií vo viacerých oblastiach – medziiným v aj oblasti POCT.

## **Metóda**

POCT definujeme ako vyšetrenie biologického materiálu:

- moča
- krvi
- slín
- potu,

ktoré je

- ľahko dostupné
- realizované pomocou jednoduchých postupov
- v tesnej blízkosti pacienta.
- čoraz viac využívajúce nanotechnológie

***Diagnosics at the point of care***



POCT sa používa

- v nemocniciach
- na ambulanciách
- doma.

V tejto súvislosti narastá význam

- konektivity
- kvality
- právneho rámca
- nanotechnológií.

## **Výsledky**

### ***Prípadová štúdia využitia nanotechnológie v rámci POCT diagnostiky v Univerzitetnej nemocnici Antwerpy***

#### Charakteristika nemocnice:

- 600 postelí
- 19 ošetrovacích staníc
- 5 chirurgických oddelení
- 22 klinických oddelení
- 5 intenzívnych jednotiek
- „Jednodňová nemocnica“
- Chest Pain Clinic

#### Ročné počty vyšetrení

*Celkový počet laboratórnych vyšetrení realizovaných v laboratóriu*

5 900 000

*POCT vyšetrenia realizované laboratóriom*

2 300 000

*POCT vyšetrenia realizované lekármi*

900 000

*Celkový počet laboratórnych vyšetrení*

9 000 000

*Cave !*

25 % všetkých laboratórnych vyšetrení je realizovaných POCT.

### ***Parametre najčastejšie využívajúce nanotechnológie v POCT diagnostike***

#### Kardiálne markery

- Troponín I
- Myoglobín
- CK-MB
- D diméry
- BNP

#### Acidobáza

#### Bilirubín a elektrolyty

#### Koagulácia

- APTT
- INR
- ACT

- Trombelastografia

### ***Okolnosti súvisiace s realizáciou POCT diagnostiky***

#### Výcvik

- Klinikov, sestier a pacientov
- Norma: ISO 22 870: smernice pre výcvik, certifikáciu a recertifikáciu užívateľov

#### Self testing a self monitoring

##### *Self testing*

výsledky sú oznamované ošetrojúcemu lekárovi, ktorý upravuje terapiu

##### *Self monitoring*

pacient si upravuje liečbu sám

#### Kontrola kvality

##### *Bias kritériá ( TE )*

- do 10 % výborné
- 10-15 % dobré
- 15-20% akceptovateľné
- nad 20 % neakceptovateľné

##### *Reproducibilita (CV )*

- Do 5 %

podľa

- American Duabetes Association
- Clinical Laboratory Improvement Amendments
- The Clinical and Laboratory Science Institute .

#### Konektivita

### **Diskusia**

V diskusii sa zameriame na problematiku implementácie POCT do klinickej praxe s cieľom definovať čo je treba zabezpečiť a ako postupovať pri dosahovaní maximálnej efektivity a eficientie POCT diagnostiky.

#### ***Audít situácie podľa kritérií***

- počet vyšetrení
- počet prístrojov
- počet výrobcov
- QC manažment
- čo sa deje s výsledkami
- expirované reagenty
- politika verifikácie šarží
- kto je zodpovedný
- celkové náklady

Štandardné závery pri podobných auditoch: „Nie je to dobré, ale mohlo by byť horšie“

Štandardné doporučenia pri podobných auditoch: simplifikácia – centralizácia – nadväznosť

- automatizácia

#### ***Pracovná skupina so zástupcami***

- laboratória
- klinikov
- sestier

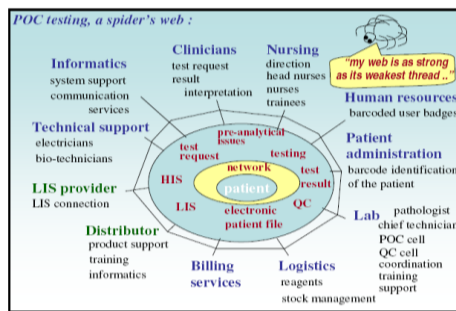
- informatikov

musí definovať požiadaviek na ideálny POCT z hľadiska

- prieskumu trhu
- vyhodnocovania systémov
- analytickej kvality ( laboratórium )
- user friendliness ( klinici ).

### **Stakeholderi rozvoja nanotechnológií a POCT diagnostiky**

- lekári
- sestry
- ľudské zdroje
- administrácia
- laboratórium
- logistika
- ekonomika
- distribútor
- LIS poskytovateľ
- technická podpora
- informatici



### **Význam konektivity**

Konektivita predstavuje absolútnu nevyhnutnosť. Manuálna registrácia výsledkov nefunguje !

Možnosti voľby sú:

- individuálne pripojenie na LIS
- skupinové pripojenie na LIS
- cez „middleware“

### **Problémy**

- Identifikácia pacienta
- Identifikácia užívateľa
- QC
- Zodpovednosť
- Tréning
- 24 hodinová technická podpora
- interferencie

### **Rozdiely: POCT a centrálné laboratórium**

10 % - 20 % rozdiely medzi centrálnym laboratóriom a POCT vyšetrením u toho istého pacienta v ten istý čas nachádzame v 60 % prípadoch.

## Závery

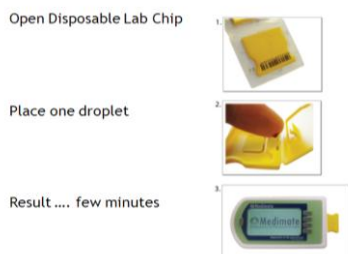
Využitie nanotechnológií v rámci POCT predstavuje celosvetový vývojový trend. POCT čoraz viac využívajúce nanotechnológie predstavuje jeden z hlavných nositeľov / predstaviteľov pojmu personalizovanej laboratórnej diagnostiky. Kvalita, konektivita a regulácia sú základným predpokladom efektívneho využitia POCT v klinickej praxi. POCT (personalizovaná laboratórna diagnostika) má potenciál dobyť trh laboratórnej diagnostiky

- v nemocnici
- na ambulancii
- doma u pacienta

lebo sa dá poskytovať bez komplikácií, jednoducho a pohodlne:

- netreba ísť do laboratória
- stačí kvapka krvi
- výsledok je za niekoľko sekúnd až málo minút.

### Make it simple



Ďalšie špecifické benefity, ktoré v dôsledku miniaturizovanej analytickej techniky POCT poskytujú sú:

- zvýšená spoľahlivosť
- prenosnosť
- nízke náklady
- implantabilita („in vivo analyzátory“).

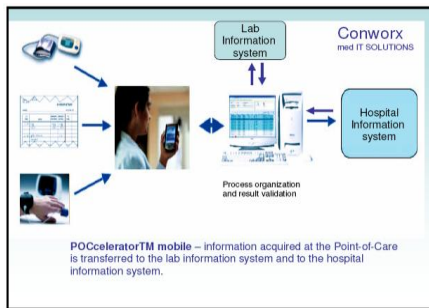


## Doporučenia

**Implementácia POCT na ktorejkoľvek úrovni si vyžaduje**

- rozsiahlu prípravu
- včasné zaangažovanie všetkých zainteresovaných
- rozsiahle skúšanie
- flexibilitu a dobrú vôľu
- konektivitu LIS / HIS

- čas naviac
- výcvik a monitoring



### ***Condition sine qua non***

Implementácie na ktorejkoľvek úrovni predstavuje vypracovanie národnej direktívy, ktorá

- definuje POCT ako klinicko laboratórne vyšetrenie moča alebo krvi pomocou jednoduchého postupu, realizované v blízkosti pacienta a za zodpovednosti kvalifikovaného laboratórneho personálu a klinického laboratória a. ( obzvlášť kritické: klinické laboratórium zodpovedné za všetky laboratórne testy – vrátane POCT ) !
- upravuje faktory prekračujúce definíciu oblasti POCT takto:
  - . znižuje používanie POCT len na situácie, v ktorých je jasne demonštrovaný benefit pre pacienta
  - . implementácia POCT je výsledkom dohody medzi klinikom a laboratóriom
  - . kompetencie a povinnosti laboratória v oblasti POCT sú rovnaké ako u laboratórnych vyšetrení a týkajú sa predanalytickej, analytickej a postanalytickej fázy
  - . je nevyhnutný monitoring a plnenie kritériá QA
  - . výučba a monitoring personálu realizujúceho POCT je v kompetencii vedúceho laboratória.

### **Literatúra**

- 1 Vivien O.M. Van Hoff, Cristel Van Campenhout: Point of Care testing: quality Issues and Future Development, Proceedings from Quality in Spotlight Meeting Antwerpen 2010
- 2 Medimate: Diagnostics at the point of care: a prefilled Lab on Chip based Electrophoresis device for point of care testing: validation results, Proceedings from Quality in Spotlight Meeting Antwerpen 2010

# INDENTATION LOAD-SIZE EFFECT IN AL<sub>2</sub>O<sub>3</sub>-SiC NANOCOMPOSITES

*Erika Csehová<sup>1</sup>, Jana Andrejovská<sup>1</sup>, Apichart Limpichaipanit<sup>2</sup>, Ján Dusza<sup>1</sup>,  
Richard Todd<sup>2</sup>*

<sup>1</sup>*Institute of Materials Research, Slovak Academy of Sciences, Watsonova 47, 040 01 Košice,  
Slovak Republic*

<sup>2</sup>*Department of Materials, University of Oxford, Parks Road, Oxford OX1 3PH,  
United Kingdom*

Corresponding author: ecsehova@imr.saske.sk

## Abstract

The indentation load-size effect (ISE) in Vickers hardness of Al<sub>2</sub>O<sub>3</sub> and Al<sub>2</sub>O<sub>3</sub> + SiC nanocomposites has been investigated and analysed using Meyer's law, proportional specimen resistance (PSR) model and modified proportional specimen resistance (MPSR) model. The strongest ISE was found for alumina. Both the PSR and MPSR models described the ISE well, but the MPSR model resulted in slightly lower true hardness values for all materials investigated. No evidence of the effect of machining stresses on the ISE has been found.

Keyword: Al<sub>2</sub>O<sub>3</sub>, SiC, Hardness, Indentation load-size effect

## 1. Introduction

During the last years it was frequently reported that the measured hardness increased with decreasing load [1, 2]. To explain this so called "indentation load/size effect - ISE" intensive research has been performed during the last decade, based on which different explanations have been advanced [3,4]. Several empirical or semi-empirical equations, including Meyer's law [5], the Hays-Kendall approach [6], the energy-balance approach [7,8], the proportional specimen resistance (PSR) model [2], etc. have been proposed for describing the variation of the indentation hardness with the applied indentation load. Probably the most widely used empirical equation for describing the ISE is Meyer's law, which gives an expression relating the load (P) and the size of indentation (d) of the form:

$$P = A.d^n, \quad (1)$$

where the exponent "n", i.e. Meyer's index, and "A" is a constant. If  $n < 2$  there is an ISE on hardness and when  $n = 2$ , the hardness is independent of the applied load

Li and Bradt in their PSR model [2], prepared on the basis of the work in [6], suggested that the specimen resistance "W", during indentation is not a constant, as was proposed by Hays and Kendall, but increases with the indentation size and is directly proportional to it according to the relationship;

$$W = a_1 d \quad (2)$$

and the effective indentation load and the indentation dimension are therefore related as follows:

$$P_{eff} = P - W = P - a_1 d = a_2 d^2. \quad (3)$$



Gong et al. [9] suggested a modified PSR model based on the consideration of the effect of the machining-induced residual stresses at the surface during the indentation in the form:

$$P = P_0 + a_1 d + a_2 d^2, \quad (4)$$

where  $P_0$  is a constant and  $a_1$  and  $a_2$  are the same parameters as in the PSR model.

The investigations up to now concerning the ISE in ceramics have focused mainly on single crystals, monolithic and composite ceramics and only a limited investigation has been carried out on ceramic nanocomposites.

The aim of the present investigation is to study the load dependence of the measured Vickers hardness of alumina – silicon carbide micro/nano composites and to describe the indentation – size effect using different models.

## 2. Experimental

The experimental materials have been prepared in the collaboration with Department of Materials, University of Oxford, Oxford, United Kingdom. Monolithic  $\text{Al}_2\text{O}_3$  and  $\text{Al}_2\text{O}_3$ -SiC nanocomposites with 5 vol% (A5) and 10 vol% (A10) of SiC particles were prepared by hot pressing in a graphite die for 30 minutes at 25 MPa in an argon atmosphere at 1700°C for the nanocomposites and 1550 °C for the pure alumina.

The microstructure and fracture surfaces were observed by scanning electron microscopy. The hardness was determined using Vickers indentation method with applied loads ranging from 1 N to 49.05 N for. The load dependence of the measured Vickers hardness of monolithic alumina and alumina – silicon carbide micro/nano composites has been investigated on different models: Meyer's law (Eq. 1), Proportional specimen resistance (PSR), (see Eq. 3) and modified PSR, according to Eq 4.

## 3. Results and discussion

Microstructure of the sample  $\text{Al}_2\text{O}_3$  consists of  $\text{Al}_2\text{O}_3$  grains separated by grain boundary phase. Increased content of SiC resulted in markedly altered microstructure. Generally, nanosized SiC particles hindered the grain growth of  $\text{Al}_2\text{O}_3$ . The sample  $\text{Al}_2\text{O}_3$ + 10vol% SiC consisted of fine microstructure. A small number of processing flaws in the form of pores or clusters of SiC grains could be identified. Location of the *intra*- and *inter*-granular inclusions within  $\text{Al}_2\text{O}_3$  matrix is shown in Fig. 1.

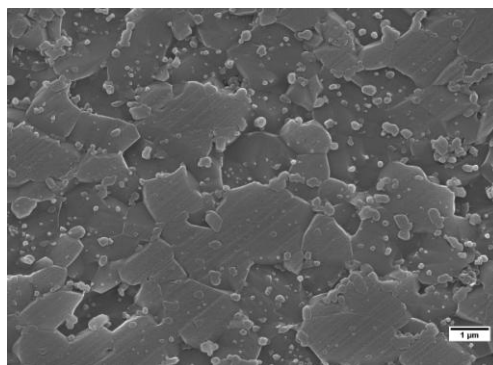
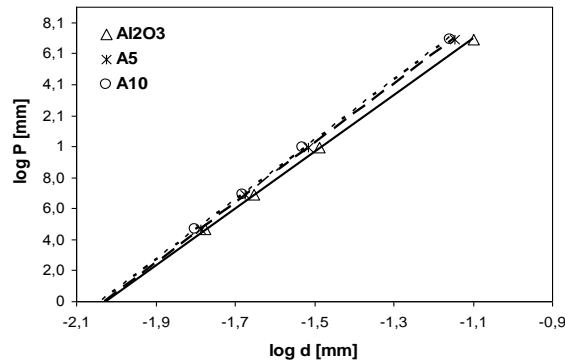


**Fig. 1.** Microstructure of the nanocomposite containing 10vol% SiC.

The macro- and micro-hardness of Al<sub>2</sub>O<sub>3</sub>/SiC composites is shown in Tab. 1. According to the results for all investigated materials the hardness increased with decreasing indentation load and with increasing volume fraction of SiC additive. The lowest hardness was found for the alumina but with decreasing load its hardness increased faster in comparison to those of the composites and at the lowest indentation load the hardness values of all materials were very similar.

| Sample                         | HV5<br>[GPa] | HV1<br>[GPa] | HV0.5<br>[GPa] | HV0.3<br>[GPa] | HV0.1<br>[GPa] |
|--------------------------------|--------------|--------------|----------------|----------------|----------------|
| Al <sub>2</sub> O <sub>3</sub> | 14.3 ± 1.0   | 17.1 ± 0.8   | 17.9 ± 1.1     | 19.3 ± 0.6     | 21.3 ± 1.7     |
| A5                             | 17.9 ± 0.4   | 19.5 ± 0.5   | 20.4 ± 1.0     | 20.5 ± 0.6     | 20.6 ± 0.5     |
| A10                            | 18.7 ± 0.3   | 20.8 ± 0.3   | 20.9 ± 0.4     | 21.2 ± 0.5     | 21.7 ± 0.5     |

**Tab. 1.** Vickers hardness of the studied materials.



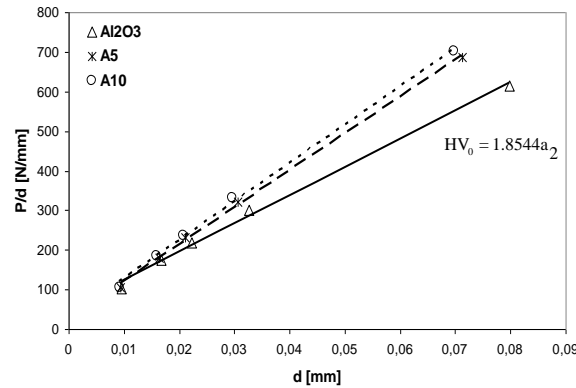
**Fig. 2.** Dependency of  $\log P$  on  $\log d$  according to Meyer's law for tested materials.

Fig. 2. illustrates the Meyer's law parameters determined by the regression analyses of the results. According to the results the most significant ISE was found in alumina ( $n = 1.83$ ) and the ISE observed in the composites ( $n = 1.92$  and  $n = 1.93$ ) was much less pronounced. These values lie within the range for "n" of 1.748 to 1.979 obtained for a variety of ceramics and glasses with indentation loads from 5 to 50N by Gong et al. [9]. Like Gong et al., we found radial cracking at the corners of the indents for all tested materials in the whole range of applied loads. Gong et al. pointed out that this may affect the hardness values obtained but since it is difficult to suppress this cracking, the extent of its influence on hardness is not clear.

The evidence here is that the nanocomposites showed smaller scatter in hardness than the pure alumina which indicates that inhomogeneities in particle distribution do not significantly affect the hardness. The better defined hardness in the nanocomposites may be a consequence of the suppression of surface microcracking in these materials by the SiC particles within the alumina grains [13, 14].

Fig. 3. shows the " $P/d-d$ " curves for the tested materials. True hardness was calculated for each material. According to Li and Bradt [2] who investigated the microhardness indentation load size effect in TiO<sub>2</sub> and SnO<sub>2</sub> single crystals, if the fact that the power-law exponent,  $n < 2$  is the result of not taking the proportional specimen resistance of the test specimen into account, then there must exist an inverse correlation between "n" and the " $a_1$ " values that describe the proportional specimen

resistance (PSR) model. This shows that both Meyer's law and the PSR model give reasonable mathematical fits to data exhibiting an ISE but there is nothing in this analysis supporting any particular physical interpretation.



**Fig. 3** Dependency of  $P/d$  on  $d$  according to the PSR model for tested materials.

The values for  $a_1$  shown in Fig. 3. are significantly smaller for the nanocomposites ( $a_1 = 28.1 \text{ N/mm}$ ,  $a_1 = 29.4 \text{ N/mm}$ ) than for the alumina ( $a_1 = 53.6 \text{ N/mm}$ ), indicating according to the physical rationalisation of the PSR model a lower „specimen resistance“ to indentation in the nanocomposites. One reason for this may be that the large, deviatoric thermal residual stresses in the nanocomposites help to initiate plastic deformation under low indentation loads. Using the Selsing formula [15] and the physical properties of the matrix (m) and particle (p),  $\alpha_m = 8.8 \cdot 10^{-6} \text{ K}^{-1}$ ,  $E_m = 380 \text{ GPa}$ ,  $\nu_m = 0.21$  and  $\alpha_p = 4.7 \cdot 10^{-6} \text{ K}^{-1}$ ,  $E_p = 490 \text{ GPa}$ ,  $\nu_p = 0.19$ , the matrix residual stresses close to the particles can be calculated to be approximately  $\sigma = -2 \text{ GPa}$  in the radial direction and  $+1 \text{ GPa}$  in the tangential direction. Stresses of this magnitude have also been confirmed experimentally [16]. A further reason for the ease of initiation of plastic deformation in the nanocomposites may be that the alumina grains of the nanocomposites are observed to contain many dislocations [10] even in the as processed condition, so there is no need to nucleate new dislocations in the early stages of indentation.

The term  $a_2$  from the linear fits in Fig. 3. describes the load independent, so called „true hardness“, which was found for  $\text{Al}_2\text{O}_3$ , A5 and A10 to be  $13.2 \text{ GPa}$ ,  $17.3 \text{ GPa}$  and  $18.0 \text{ GPa}$ , respectively.

Gong et al [9] investigated the ISE in ceramics with fracture toughness from  $0.8 \text{ MPam}^{0.5}$  to  $12.4 \text{ MPam}^{0.5}$ . They found that for some ceramics the PSR model does not provide a satisfactory explanation of the ISE and offered a modified PSR model to solve this problem, see equation 4. The term  $P_0$  in this model was rationalised by Gong et al. in relation to the residual surface stresses in the test specimen associated with the machining and polishing of the samples prior to testing.

In Fig. 4. the relationship between  $P$  and the indentation size,  $d$ , is illustrated in the form of polynomial curves with the calculated parameters of the modified PSR model. The values for  $a_1$  are for the nanocomposites A5 and A10 ( $a_1 = 65.4 \text{ N/mm}$ ,  $a_1 = 81.7 \text{ N/mm}$ ) respectively, for the alumina is  $a_1 = 108.2 \text{ N/mm}$ . The correlation is very good, although the introduction of an extra adjustable parameter ( $P_0$ ) is bound to lead to improved fitting, whatever the correct physical explanation of the ISE. In the present case, the values of  $P_0$  were negative for the monolithic alumina and for the composites too. There is therefore no systematic trend occurred which may relate to microstructure or surface residual stresses from machining.

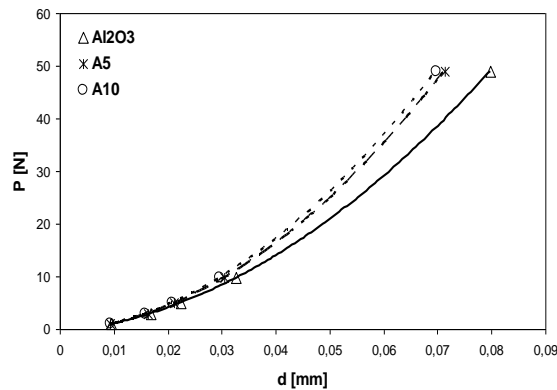


**Fig. 4** Dependency of  $P$  on  $d$  for tested materials according to the MPSR model.

The MPSR model results in slightly lower „true hardness“ values of  $11.9 \text{ GPa}$ ,  $16.3 \text{ GPa}$  and  $16.7 \text{ GPa}$ , for the  $\text{Al}_2\text{O}_3$ , A5 and A10 ceramics, respectively, although the trend in hardness with SiC addition is the same as was found for the PSR.

#### 4. Conclusion

The strongest ISE was found for alumina with a Meyer's index of  $n = 1.83$ . The lower ISE for the nanocomposites was attributed to the high thermal stresses and pre-existing dislocation distributions in these materials. The PSR model can be used to analyze the ISE observed in all of tested materials. According to the modified PSR model results, in comparison with Vickers hardness exhibits lower values due to cracking. No evidence was found for the influence of machining stresses on the ISE and it is likely that the introduction of  $P_0$  in the modified PSR model improves the fit to results mainly by providing an extra adjustable variable rather corresponding to a simple physical phenomenon.

#### Acknowledgements

This work was partly supported by APVV LPP 0174-07 and „Centre of Excellence of Advanced Materials with Nano- and Submicron- Structure“, which is supported by the Operational Program “Research and Development” financed through European Regional Development Fund.

#### References

- [1] Clinton, D., J., Morell, R.: *Mater., Chem. Phys.* 17 (1987) 461.
- [2] Li, H., Bradt, R., C.: *J. Mater. Sci.*, 28 (1993) 917.
- [3] Bückle, I., H., *Metall. Rev.*, 4 (1959), pp. 49-100.
- [4] Mason, W., Johnson, P. F., Varner, J. R., *J. Mater. Sci.*, 26 (1991) 6576.
- [5] Tabor, D., *The hardness of Metals*, Oxford University Press, Oxford, UK, 1951
- [6] Hays, C., Kendall, E. G.: *Metall.*, 6 (1973) 275.
- [7] Froehlich, F., Grau, P., and Grellmann, W., *Phys. Status Solidi*, 42 (1977) 79.
- [8] Quinn, J., B., Quinn, G., D.: *J. Mater. Sci.*, 32 (1997) 4331.

- [9] Gong, J., Wu, J., Guan, Z.: *J. Eur. Ceram. Soc.*, 19 (1999) 2625.
- [10] Niihara, K., *J. Ceram. Soc. Jpn.*, 99(10) (1991) 974.
- [11] Sternitzke, M, *J. Eur. Ceram. Soc.*, 17 (1997) 1061.
- [12] Walker, C. N., Borsa, C.E., Todd, R. I., Davidge, R. W. and Brook, R. J.,  
*British Ceramic Proc.* 53 (1994) 249
- [13] Ortiz Merino, J. L. and Todd, R.I., *Acta Mater.* 53 (2005) 3345
- [14] Limpichaipanit, A. and Todd, R.I., *J. Eur. Ceram. Soc.* 29 (2009) 2841
- [15] Selsing, J., *J. Am. Ceram. Soc.*, 44 (1961) 419.
- [16] Ortiz Merino, J.L. and Todd, R.I., *J. Eur. Ceram. Soc.* 23 (2003) 1779
- [17] Peng, Z., Gong, J., Miao, H, *J. Eur. Ceram. Soc.*, 24 (2004) 2193.

# DETERMINATION OF PARTICLE SHAPE AND SIZE DISTRIBUTION OF MODEL TYPES OF NANOMATERIALS

***Edita Bretšnajdrová<sup>1</sup>, Ladislav Svoboda<sup>1</sup>, Jiří Zelenka<sup>2</sup>***

*<sup>1</sup>University of Pardubice, Faculty of Chemical Technology, Department of Inorganic Technology, Nám. Čs. Legii 565, 532 10 Pardubice, Czech Republic*

*<sup>2</sup>Synpo, akciová společnost, S. K. Neumanna 1316, 532 07 Pardubice, Czech Republic*

Corresponding author: edita.bretsnajdrova@student.upce.cz

## 1 Introduction

At present great attention is given to study of preparation and properties of various nanomaterials usable in many applications. They are utilized in varied fields of human activity – e.g. in electronics, medicine, paint industry etc. Except detailed chemical structure, such nanoparticle properties as shape and size distribution are fundamental to the given application. To measure these parameters various methods are used, e.g. transmission electron microscopy (TEM), atomic force microscopy (AFM), acoustic spectrometry, methods based on the light scattering and X-ray disc centrifuge system.

All above-mentioned methods were used in this work to characterize particles of two selected model types of nanomaterials – colloidal silica and sodium montmorillonite. Silica represents a material with spherical particles. Tabular shapes are typical for montmorillonite materials.

Experiments proved that methods used to measure particle size distribution based on the light scattering require very diluted dispersions. But, on the other hand, these conditions can affect the particle size distribution due to agglomeration or deagglomeration of the particles. For these reasons methods working with concentrated suspensions, without a great dilution, are more suitable to get correct results for such colloidal systems, for example acoustic spectrometry and X-ray disc centrifuge system. To obtain information on the shape of particles TEM and AFM methods were used.

Merits and limitations of the individual methods used to evaluation of nanoparticles of various types are discussed in this work.

## 2 Materials

### 2.1 Silica

- Bindzil cc 30, Eka Chemicals AB, Sweden, dispersion of silica nanoparticles, 30% solution in water, particle size 7 nm, sterically stabilized.
- Bindzil 30/360, Eka Chemicals AB, Sweden, dispersion of silica nanoparticles, 30% solution in water, particle size 7 nm, electrostatically stabilized.

### 2.2 Montmorillonite

- Cloisite Na<sup>+</sup>, Southern Clay Products, Inc., USA, powdery clay, CEC 90 meq/100g.

## 3 Experimental

### 3.1 Ultrasound spectroscopy

The ultrasound based technique is suitable for characterizing heterogeneous solid in liquid or liquid in liquid colloidal systems. This method is suitable for concentrated solutions; it is reliable in range from 5% to 50%. We have used equipment DT-1200 (Dispersion technology,

USA). Range of measurement of particle size is from 0,005  $\mu\text{m}$  to 1000  $\mu\text{m}$  and frequency range is from 1 to 100 MHz.

### **3.2 *Dynamic light scattering***

The technique of laser diffraction is based around the principle that particles passing through a laser beam will scatter light at an angle that is directly related to their size. Particle size distribution measurement was carried out by dynamic light scattering using two types of instruments – Mastersizer 2000 MU and 90 Plus/BI-MAS.

Mastersizer 2000 MU (Malvern, United Kingdom) measures materials from 0,02  $\mu\text{m}$  to 2000  $\mu\text{m}$ . This instrument is suitable for the measurement of emulsion, suspension and dry powders.

90 Plus/BI-MAS (Brookhaven Instruments Corporation, USA) is an automatic particle sizer designed for use with either concentrated suspensions of small particles or solutions of macromolecules. Sizes from 2 nm to 3  $\mu\text{m}$  can be measured.

### **3.3 *X-ray disc centrifuge system***

For measurement of particle size the X-ray disc centrifuge system (Brookhaven Instruments Corporation, USA) was used. XDC method allows you to make measurements in either a centrifugal or a gravitational field. X-rays from a low power X-ray tube are passed through the disc. The intensity of the beam is attenuated in proportion to the concentration of the suspension through which it passes. The intensity of the transmitted beam is measured with a detector consisting of a scintillation counter whose output is recorded by the computer as a function of time. For a homogeneous suspension, the attenuation of the X-ray beam is proportional to the mass concentration of the suspension at the measurement radius.

### **3.4 *AFM***

A Solver Pro M Atomic Force Microscope (NT-MDT, Russia) was used in tapping mode (semi-contact) to produce three-dimensional images of the surface. High resolution „golden” silicon cantilever NSG-10 (Au coating, curvature radius 10 nm and cone angle less than  $22^\circ$ ) were used for all measurements. Set point was adjusted on 50% of a free oscillation. Scan sizes required to evaluate the distribution of particles was 500x500 nm to several microns depending on variation of particles size.

### **3.5 *TEM***

A drop of the water-diluted suspension was put on a microscopic grid covered by ultra thin carbon film and observed directly with TEM Tecnai G2 Spirit Twin (FEI, USA).

## **4 Results**

### **4.1 *Silicas***

Two types of commercial silicas were tested (Bindzil cc 30 and Bindzil 30/360). These silicas are stabilized different way. While Bindzil cc 30 is sterically stabilized, Bindzil 30/360 is stabilized electrostatically. The effect of silica concentration on zeta potential and particle size was studied for both type of stabilization. The variety of silica concentrations were prepared by dilution of original samples. Type of stabilization has crucial effect on silica concentration dependence of zeta potential (Fig.1).

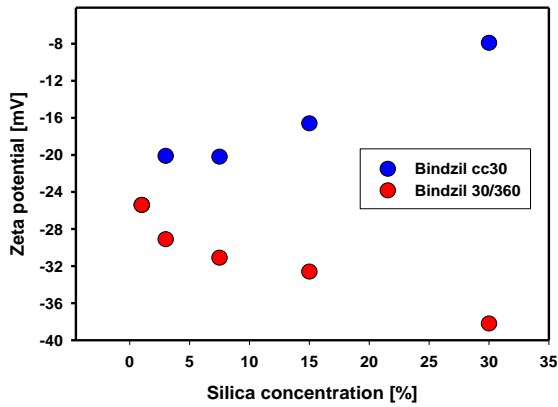


Figure 1: Dependence of zeta potential on silica concentration

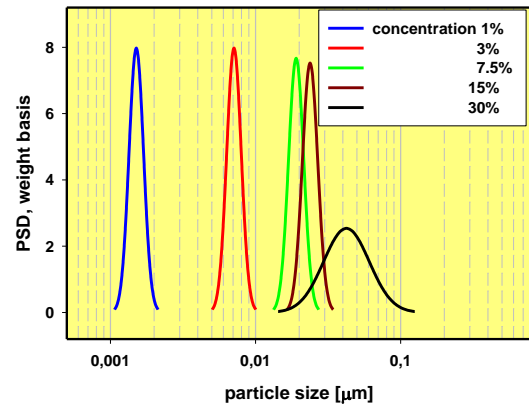


Figure 2: Particle size distribution on silica concentration

The concentration of silica has effect on particle size and particle size distribution. Example for Bindzil cc 30 is in Fig.2.

Original sample of Bindzil cc 30 has relatively broad particle size distribution. Mean value of particle size is about 40 nm. Measured value is higher than value cited by producer. Presence of bigger formations was confirmed by transmission electron microscopy (Fig.3).

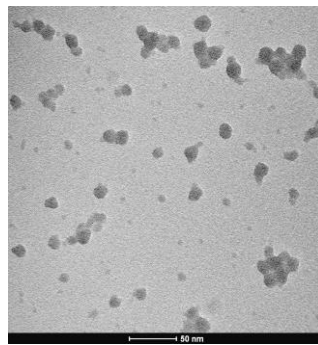


Figure 3: TEM photo of original sample Bindzil cc 30

#### 4.2 Montmorillonite

Zeta potential of water-based dispersion of sodium montmorillonite was influenced by filler concentration (Fig.4).

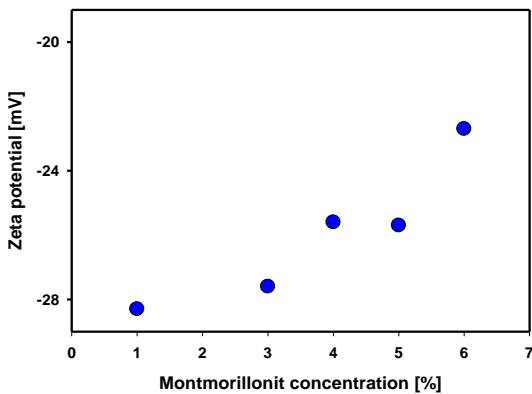


Figure 4: Dependence of zeta potential on montmorillonite concentration

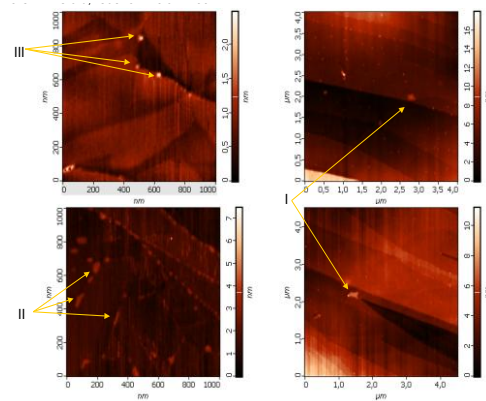


Figure 5: AFM photo of sodium montmorillonite



The particles with different shape and dimension were observed by means of different techniques (TEM, AFM). Results from AFM are in Fig 5.

Pentagon particles with particle size about 200 nm can be observed in section I of Fig. 5. Lengthwise formation with highest dimension 100 nm can be seen in part II of Fig. 5. Round particles with diameter 30 nm are in part III. Thickness of all studied particles is practically the same - about 1 nm.

## **5 Conclusions**

Type of silica particle stabilization influenced behaviour of colloidal solutions during dilution (particle size and zeta potential changes). All used methods give similar results. Bigger particles (aggregates primary particles) were observed by means of AFM and TEM. These aggregates were broken up by dilution of original samples.

Commercial sodium montmorillonite is compound from elements different shapes and sizes. There are lengthwise formations, circular and pentagonal particles.

## **6 References**

1. Kosmulski M., Dahlsten P.: *Colloids and Surfaces* 291, 212-218 (2006).
2. Pierre A.C.: *Journal of Materials Science* 32, 2937-2947 (1997).
3. Yukselen Y., Kaya A.: *Water, Air and Soil Pollution* 145, 155-168 (2003).

*This work has been supported by the projects FT-TA3/055 and FT-TA4/074 of the Ministry of Industry and Trade of the Czech Republic and has been supported from the resources of the research intention MSM 0021627501.*


# CARBON NANOTUBE BRIDGES GROWN ON ALUMINOSILICATES BY HOT FILAMENT CVD PROCESS

*Katarína Pastorková<sup>1</sup>, Magdaléna Kadlečíková<sup>2</sup>, Filip Lazišťan<sup>2</sup>, Michal Kolmačka<sup>2</sup>, Karol Jesenák<sup>1</sup>, Juraj Breza<sup>2</sup>, Miroslav Michalka<sup>3</sup>*


<sup>1</sup>Faculty of Natural Sciences, Department of Inorganic Chemistry, Comenius University, Mlynská dolina, 842 15 Bratislava, Slovakia

<sup>2</sup>Faculty of Electrical Engineering and Information Technology, Department of Microelectronics, Slovak University of Technology, Ilkovičova 3, 812 19 Bratislava, Slovakia

<sup>3</sup>International Laser Centre, Ilkovičova 3, 812 19 Bratislava, Slovakia



## CARBON NANOTUBE BRIDGES GROWN ON ALUMINOSILICATES BY HOT FILAMENT CVD PROCESS



*Katarína Pastorková<sup>1</sup>, Magdaléna Kadlečíková<sup>2</sup>, Filip Lazišťan<sup>2</sup>, Michal Kolmačka<sup>2</sup>, Karol Jesenák<sup>1</sup>, Juraj Breza<sup>2</sup>, Miroslav Michalka<sup>3</sup>*


<sup>1</sup>Faculty of Natural Sciences, Department of Inorganic Chemistry, Comenius University, Mlynská dolina, 842 15 Bratislava, Slovakia  
<sup>2</sup>Faculty of Electrical Engineering and Information Technology, Department of Microelectronics, Slovak University of Technology, Ilkovičova 3, 812 19 Bratislava, Slovakia  
<sup>3</sup>International Laser Centre, Ilkovičova 3, 812 19 Bratislava, Slovakia

### INTRODUCTION


The fabrication of well-defined and organized arrays of CNTs, in sufficient quantities and at a low cost, is of high importance, due to their unique properties and promising applications. Many parameters can affect the nature of the carbon deposits in the resulting material. In particular, the choice of the metal particles and the catalyst support may strongly influence the structure and the morphology of the carbon deposits.

In this work we studied influence of the type catalytic support upon the morphology, quality and structure of the final products especially carbon nanotube bridges. Information regarding the carbon nanotubes ability to form of bridges could be important for the manufacture of CNTs-based nanodevices or for improvement of mechanical properties of nanocomposites.

### EXPERIMENTAL

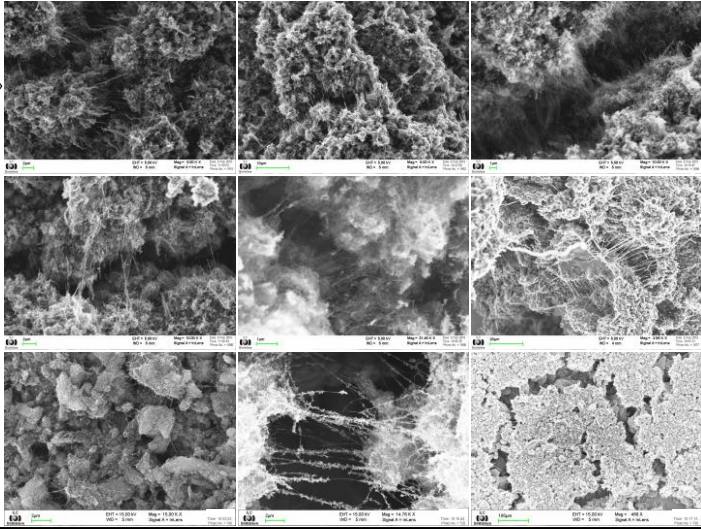


We used natural aluminosilicates (namely: montmorillonite, zeolite-clinoptilolite) as a catalytic support for the metal catalytic centers (Fe nanoparticles). The metal impregnated samples were prepared by immersing appropriate aluminosilicate into aqueous solution of  $\text{FeCl}_3 \cdot 6\text{H}_2\text{O}$  or  $\text{Fe}(\text{NO}_3)_3 \cdot 9\text{H}_2\text{O}$  with 0,04 M concentration. The suspensions were stirred for 12 h. The suspensions were finally deposited on Si wafer by sedimentation and allowed to quick dry by infrared lamp.



Deposition of CNTs was carried out in the HF CVD reactor, where the precursor is activated by five tungsten filaments heated up to 2200°C. The working atmosphere was a mixture of methane and hydrogen. The pressure and temperature during deposition were 3000 Pa and  $\approx 600^\circ\text{C}$  respectively. The growth time was 30 min.

### RESULTS

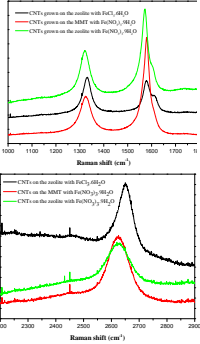


SEM images of the CNT bridges grown on Fe-montmorillonite pretreated with  $\text{Fe}(\text{NO}_3)_3 \cdot 9\text{H}_2\text{O}$

SEM images of CNT bridges grown on Fe-zeolite pretreated with  $\text{Fe}(\text{NO}_3)_3 \cdot 9\text{H}_2\text{O}$

SEM images of CNT bridges grown on Fe-zeolite pretreated with  $\text{FeCl}_3 \cdot 6\text{H}_2\text{O}$

#### Raman spectra of the CNTs grown on Fe-aluminosilicates



— CNTs grown on the zeolite with  $\text{FeCl}_3 \cdot 6\text{H}_2\text{O}$   
— CNTs grown on the MBT with  $\text{Fe}(\text{NO}_3)_3 \cdot 9\text{H}_2\text{O}$   
— CNTs grown on the zeolite with  $\text{Fe}(\text{NO}_3)_3 \cdot 9\text{H}_2\text{O}$

— CNTs on the zeolite with  $\text{FeCl}_3 \cdot 6\text{H}_2\text{O}$   
— CNTs on the MBT with  $\text{Fe}(\text{NO}_3)_3 \cdot 9\text{H}_2\text{O}$   
— CNTs on the zeolite with  $\text{Fe}(\text{NO}_3)_3 \cdot 9\text{H}_2\text{O}$

### CONCLUSION

MWNTs were obtained both on Fe-zeolite and Fe-montmorillonite. The SEM images showed carbon nanotube bridges. The nanotubes were bridging-cross both single parts of aluminosilicates and micro-cracks, which had been formed during quick drying on aluminosilicate layers. The carbon nanotubes (CNTs) formed a three-dimensional CNTs/aluminosilicate network. The length of these nanotubes was in a range from several nm to nearly 10  $\mu\text{m}$ . Diameters of the grown MWNTs were in a narrow range but the nanotubes contain also other forms of carbon. Raman spectroscopy revealed the presence of amorphous carbon on the surface of MWNTs and moreover, the position of the D and G bands are characteristic for CNTs. Consequently, the forming carbon nanotube bridges in a material can provide promising way to produce new nanocomposites with improved mechanical properties.

### ACKNOWLEDGEMENT

This work has been supported by grant VEGA 1/0746/09 of Ministry of Education of the Slovak Republic and has been received additional support by grants UK/273/2009 and UK/534/2010

